12

Multifunctional Materials

**Sia Nemat-Nasser, Syrus Nemat-Nasser, Thomas Plaisted,
Anthony Starr, and Alireza Vakil Amirkhizi**

CONTENTS

12.1 Introduction 309
12.1.1 Multifunctional Concepts 310
12.2 Multifunctional Composites 311
12.2.1 Electromagnetic Functionality 312
12.2.1.1 Thin-Wire Plasmonic Composites 312
12.2.1.2 Coiled Wire Plasmon Media Composites 314
12.2.1.3 Braided Composite Manufacturing 318
12.2.1.4 Controlling the Effective Magnetic Permeability 321
12.2.1.5 Negative Refractive Index Composites 323
12.2.2 Heating Functionality 324
12.2.2.1 Simulation and Testing 324
12.2.3 Healing Functionality 328
12.2.3.1 Polymer Healing 329
12.2.3.2 Thermo-Reversibly Cross-Linked Polymer 329
12.2.3.3 Healing Experiments 330
12.2.3.4 Healing Summary 332
12.2.4 Sensing Functionality 332
12.2.4.1 Integrating Sensing into Composites 333
12.2.4.2 Sensor Communications and Power 333
12.2.4.3 Mechanical Integration 333
12.2.4.4 Data Management 335
12.2.4.5 Preliminary Results 335
12.2.4.6 Sensors for Structural Health Monitoring 337
12.3 Summary 337
Notes 338
References 338

12.1 INTRODUCTION

Multifunctional structural materials possess attributes beyond the basic strength and stiffness that typically drive the science and engineering of the material for structural systems. Structural materials can be designed to have integrated electrical, magnetic, optical, locomotive, power generative, and possibly other functionalities that work in synergy to provide advantages that

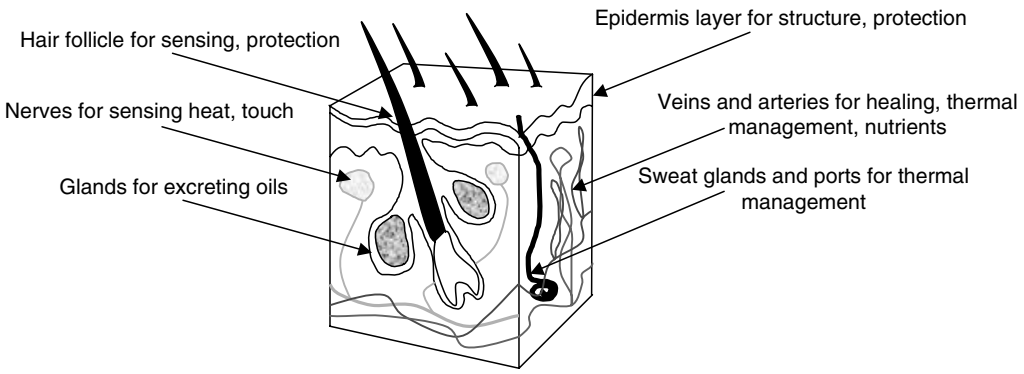

Figure 12.1 Illustration of the many integrated functions within the human skin.

reach beyond that of the sum of the individual capabilities. Materials of this kind have tremendous potential to impact future structural performance by reducing size, weight, cost, power consumption, and complexity while improving efficiency, safety, and versatility.

Nature offers numerous examples of materials that serve multiple functions. Biological materials routinely contain sensing, healing, actuation, and other functions built into the primary structures of an organism. The human skin, for instance (see Figure 12.1), consists of many layers of cells, each of which contains oil and perspiration glands, sensory receptors, hair follicles, blood vessels, and other components with functions other than providing the basic structure and protection for the internal organs. These structures have evolved in nature over eons to the level of seamless integration and perfection with which they serve their functions. Scientists now seek to mimic these material systems in designing synthetic multifunctional materials using physics, chemistry, and mathematics to their advantage in competing with the unlimited time frame of nature's evolutionary design process. The multifunctionality of these materials often occurs at scales that are nano through macro and on various temporal and compositional levels.

12.1.1 Multifunctional Concepts

In recent years, wide arrays of multifunctional material systems have been proposed. Each of these systems has sought to integrate at least one other function into a material that is capable of bearing mechanical loads and serves as a structural material element. Researchers at ITN Energy Systems and SRI International have integrated a power-generating function into fiber-reinforced composites (Christodoulou and Venables, 2003). Individual fibers are coated with cathodic, electrolytic, and anodic forming layers to create a battery. The use of the surface area of fibers as opposed to that of a foil in a thin film battery allows greater energy outputs, measured on the order of 50 Wh/kg in a carbon fiber-reinforced epoxy laminate. These batteries may be deposited on various substrates, including glass, carbon, and metallic fibers. This research and many others, including our own research, have been supported by DARPA under the first generation of Synthetic Multifunctional Materials Initiative (Figure 12.2).

Other power-generating schemes integrated into structural composites have been proposed, where the composite structure is consumed to generate power after its structural purpose is complete (Joshi et al., 2002; Thomas et al., 2002; Baucom et al., 2004; Qidwai et al., 2004). Physical Sciences Inc. have incorporated oxidizers into thermoplastic matrix composites and demonstrated significant energy output from directly burning the material (Joshi et al., 2002). Such a material would be useful for instance in a space application, where weight saving is critical, and structures required only for launch could provide an energy source once the structure is no longer needed.

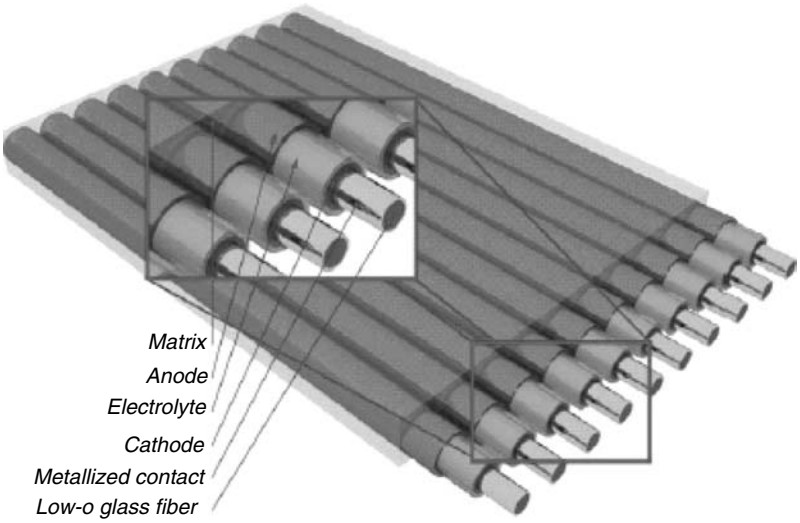

Figure 12.2 ITN Powerfiber with simultaneous battery and structure functionalities.

The integration of sensing into materials has made many advances in recent years. Much of the research has been conducted under the context of Structural Health Monitoring, or SHM. In line with the overall theme of this book, researchers seek to make a material sense its environment, feel internal damage, and signal an alert that repair is needed, essentially mimicking the behavior of biological organisms. Later in this chapter we provide an approach to integrating sensing into composite materials. For a comprehensive overview of the field, the reader is directed to a recent review paper on the subject (Mal, 2004).

This brief introduction to multifunctional materials only scratches the surface of the various multifunctional concepts developed to date. The remaining sections of this chapter will detail a further example of a multifunctional material under development at University of California, San Diego (UCSD), in the first author's laboratories. The functionalities of this material include integrated structural, electromagnetic, thermal, healing, and sensing capabilities. While this material in no way encompasses all of the possible functionalities that may be integrated into a material, it offers an example of how such an integration may be achieved while maintaining the structural integrity of the overall material. Particular attention is given to the interplay and resulting synergy between the various elements that contribute these functionalities.

12.2 MULTIFUNCTIONAL COMPOSITES

We focus on the issues that relate to integrating multiple functions into fiber-reinforced polymers to create composites with basic structural attributes that can also perform other functions. We discuss various methods that have been used to control the mechanical, electromagnetic (EM), and thermal properties of the material, while introducing self-healing, and environmental-sensing and prognostic capabilities into the material. The polymer matrix of these composites has the ability to covalently heal microcracks at rates that can be facilitated by moderate heating through thin conductors which are also used to control the EM properties of the material. The same conductors can also be used to create sensor-integrated electronic networks within the composite, capable of sensing, and local and global communications and decision making.

12.2.1 Electromagnetic Functionality

Recent advances in electromagnetic (EM) *metamaterials* have provided an opportunity to change and tune the dielectric constant as well as the index of refraction of the material over a range of useful frequencies. Electromagnetic metamaterials are artificially structured media with unique and distinct EM properties that are not observed in naturally occurring materials. A variety of metamaterials with striking EM properties have been introduced, most notably those with a negative refractive index (NRI). NRI is associated with a medium of simultaneously negative electric permittivity, ε and the magnetic permeability, μ. There are no known conventional materials with such exceptional properties. Recently, Smith et al. (2000a,b) at UCSD have produced a medium with effective ε and μ that are measured to be simultaneously negative. Later, Smith et al. performed a Snell's law experiment on a similar metamaterial wedge sample, and demonstrated the negative refraction of a microwave beam (Shelby et al., 2001). Thus they showed that their medium does indeed possess an NRI, that is, it is a negative index material (NIM). Such a property has been hypothesized by Veselago who termed the medium "left-handed" (Veselago, 1968). The work on controlling the dielectric constant and producing negative ε and μ has been discussed by Smith et al. (Smith et al., 2002, 2003, 2004a,b,c; Kolinko and Smith, 2003; Pendry et al., 2003). However, until recently, the NIMs produced have been experimental samples, suitable only for proof-of-concept demonstrations.

Based on the calculation of the effective EM properties of a medium containing periodically distributed very thin conducting wires and electric resonators, the authors at UCSD have introduced into structural composites electromagnetic enhancements in the form of tunable index of refraction, radio frequency (RF) absorption, and when desired, a negative index of refraction (Starr et al., 2004). Such properties are the result of embedding periodic metal scattering elements into the material to create an *effective medium* response over desired RF frequency ranges. We have identified two wire architectures, namely thin straight wire arrays and coiled wire arrays, that are suitable for direct integration into fiber-reinforced composites (Nemat-Nasser et al., 2002). These arrays act as inductive media with a plasma-like response to control the electric permittivity. As a result, the dielectric constant may be tuned to negative or positive values. Such a medium may be used as a window to filter electromagnetic radiation. When the dielectric constant is negative, the material does not transmit incident radiation. As the dielectric constant approaches to and exceeds the *turn-on frequency*, the incident EM radiation is transmitted through the composite. Furthermore, over a desired frequency range, the dielectric constant may be tuned to match that of the surrounding environment. For instance, the dielectric constant may be tuned to match that of air, with a dielectric constant of unity, such that incident radiation does not experience a difference when encountering the composite.

12.2.1.1 Thin-Wire Plasmonic Composites

The ionosphere is a dilute plasma. Many artificial dielectrics are plasma analogs. In 1996, Pendry et al. suggested an *artificial plasmon medium* composed of a periodic arrangement of very thin conducting wires, predicting a plasma frequency in the microwave regime, below the diffraction limit. Recently, other researchers have presented examples of artificial plasmon media at microwave frequencies (Smith et al., 1999). The dielectric constant κ of a dilute neutral plasma is given by

$$\kappa = 1 - \left(\frac{f_{\mathrm{p}}}{f}\right)^2 \tag{12.1}$$

where f_{p} is the plasma frequency and f is the electromagnetic excitation frequency. This parameter must be evaluated empirically for any configuration, but analytical and numerical results can

be easily used for design purposes. Pendry et al. provide the following analytical formula for thin wire media[1]:

$$f_{\mathrm{p}} = \frac{c_0}{d}\sqrt{\frac{1}{2\pi(\ln\left(\frac{d}{r}\right) - \frac{1}{2}(1 + \ln\pi))}} \tag{12.2}$$

where c_0 denotes the speed of light in vacuum, d is the lattice spacing, and r is the radius of the wires (Pendry et al., 1996). Straight wire arrays, such as those shown in Figure 12.3, are designed such that the radius of the wires is very small compared to the lattice spacing, so that the wavelength of the electromagnetic excitation frequency is large compared to the lattice size. For the medium to behave as a plasma at microwave frequencies, for instance, the wire radius must be on the order of tens of micrometers and spaced on the order of centimeters. To integrate such electromagnetic

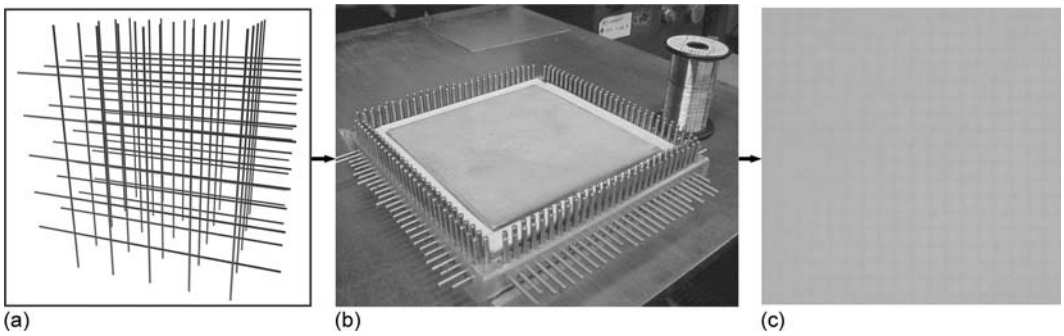

Figure 12.3 (Top) Schematic of two-dimensional thin wire array. One hundred micrometer wires are periodically embedded between composite laminates with layup jig to yield a processed fiberglass/epoxy laminate with array visible inside. (Bottom) Laminating hot presses for processing composite panels.

designs into materials, one needs a periodic material that can accommodate the arrangement of the wire elements. Fiber-reinforced polymer composites facilitate such arrangements due to the natural periodicity of their fiber and laminate construction. The arrangement of fibers within each layer provides flexibility in orientation, spacing, and geometry of the conducting wire elements. Each layer may contain elements with orientation in only one direction, as in a uni-directional laminate, or the elements may be woven such that each layer has bi-directional elements. Variation of the spacing of these elements in the thickness (z) dimension of the material is controlled by the sequence in which laminates are stacked to form the laminate.

As an example, we have introduced arrays of thin, straight wires into various types of composite materials. Composite panels were made by hand-layup of preimpregnated woven fabric (prepreg). The samples varied in the type of host material, wire diameter, and number of electromagnetic layers. Host materials included E-glass fibers impregnated with epoxy resin, Spectra® (Honeywell UHMW polyethylene) fibers impregnated with vinyl ester resin, and quartz fibers impregnated with cyanate ester resin, chosen for their mechanical attributes and favorable dielectric characteristics. The dielectric constant of epoxy/E-glass was 4.44 at microwave frequencies with a loss tangent of 0.01, and that of vinyl ester/Spectra was 2.45 with a loss tangent of 0.002. Cyanate ester/quartz provided the best overall electromagnetic characteristics with a dielectric constant of 3.01 and a loss tangent of 0.001, where a low dielectric constant and loss tangent are preferable for optimal microwave transmission. The fiber volume fraction for each material was about 60%. The frequency at which the panels behave as plasma depends upon the dimensions of the embedded wire array. Numerical simulations were performed to predict the necessary array for plasma response in the microwave regime. In making each panel, copper wire of 75 or 50 μm diameter was strung across a frame to form the desired pattern and was subsequently encased in layers of prepreg. Panels were processed at elevated temperature and pressure to cure the resin and form the solid composite as shown in Figure 12.3. Electromagnetic characterization was performed to extract the effective material properties through measurements in an anechoic chamber that we developed in the Physics Department of UCSD. Additional characterizations have been performed on a focused beam electromagnetic system in the first author's laboratories, CEAM (Center of Excellence for Advanced Materials), as is discussed in connection with Figure 12.13 later on.

Representative dispersion relations of the dielectric constant in the microwave regime for each of these panels are given in Figure 12.4, comparing analytical and numerical predictions with the experimental results. The graphs in this figure show the characteristic trend of changing the dielectric constant from negative to positive values as a result of the plasmon media in a composite panel of each type. Results for the different host materials show similar behavior, though the turn-on frequency is shifted depending on the dielectric constant of the host material and the wire diameter and spacing. Moreover, the results show that a host material with a lower dielectric constant provides a wider bandwidth over which the dielectric constant of the free space can be matched (Plaisted et al., 2003 b).

12.2.1.2 Coiled Wire Plasmon Media Composites

As an alternative to processing thin wires into composites, we may incorporate thicker, more robust wires in the form of coiled arrays. By proper design of the coil geometry, various degrees of inductance may be achieved with thicker wires as compared with the thin straight wires. Textile braiding of reinforcing fibers with wire is an ideal method to integrate the coil geometry into the composite. The braiding process interlaces two or more yarns to form a unified structure. Our process uses a two-dimensional tubular braiding machine, as shown in Figure 12.5, which operates in a maypole action, whereby half of the yarn carriers rotate in a clockwise direction, weaving in and out of the remaining counter-rotating carriers. This action results in a two-under two-over braid pattern. Each yarn makes a helical path around the axis of the braid to create a uniform coil. To integrate the wire coil into such a structure, we simply replace one of the fiber

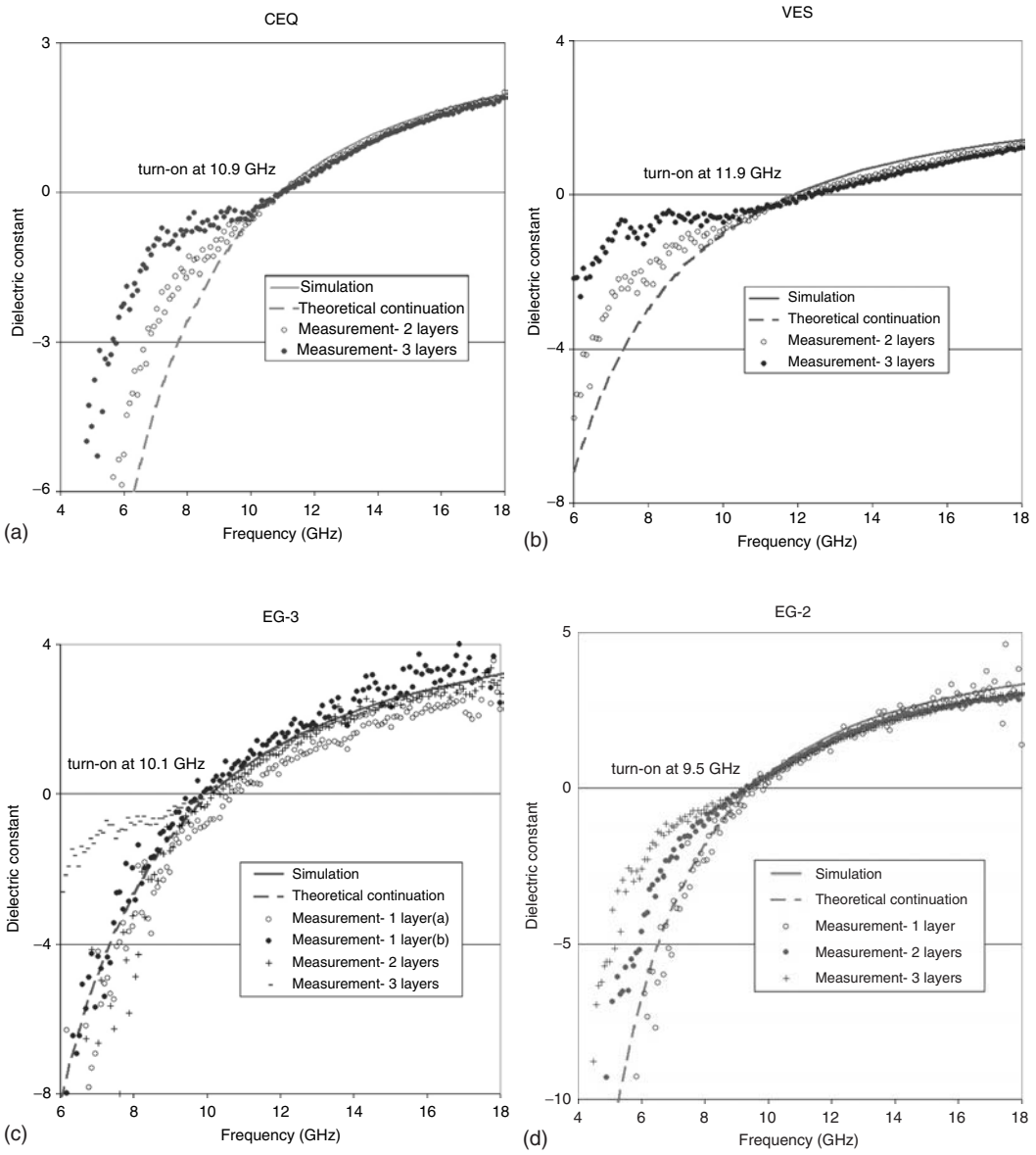

Figure 12.4 Numerical and experimental characterization of the thin-wire EM composite samples. Data for panels made of the same host composite material and wire diameter are displayed in one chart since their numerical simulations are identical. "Turn-on" indicates the transition between the stop-band and pass-band, or the frequency above which the material transmits electromagnetic radiation. (a) 50 μm (0.002 in.) diameter wires embedded in cyanate ester/quartz composite. (b) 50 μm diameter wires embedded in vinyl ester/Spectra composite. (c) 75 μm (0.003 in.) diameter wires embedded in epoxy/E-glass composite (two single layer samples were manufactured and measured for this case). (d) 50 μm diameter wires embedded in epoxy/E-glass composite.

carriers with a wire carrier. A comprehensive description of the textile braiding process is given by (Ko et al. 1989 and Ko 2001). Modeling of the mechanical properties has also been developed for textile braids (see e.g., Cox et al., 1994; Naik, 1995; Xu et al., 1995; McGlockton et al., 2003; Yang et al., 2003).

Braiding wire with the reinforcing fibers results in an electromagnetic element with uniform geometry that maintains its shape under considerable handling and other processing conditions. The

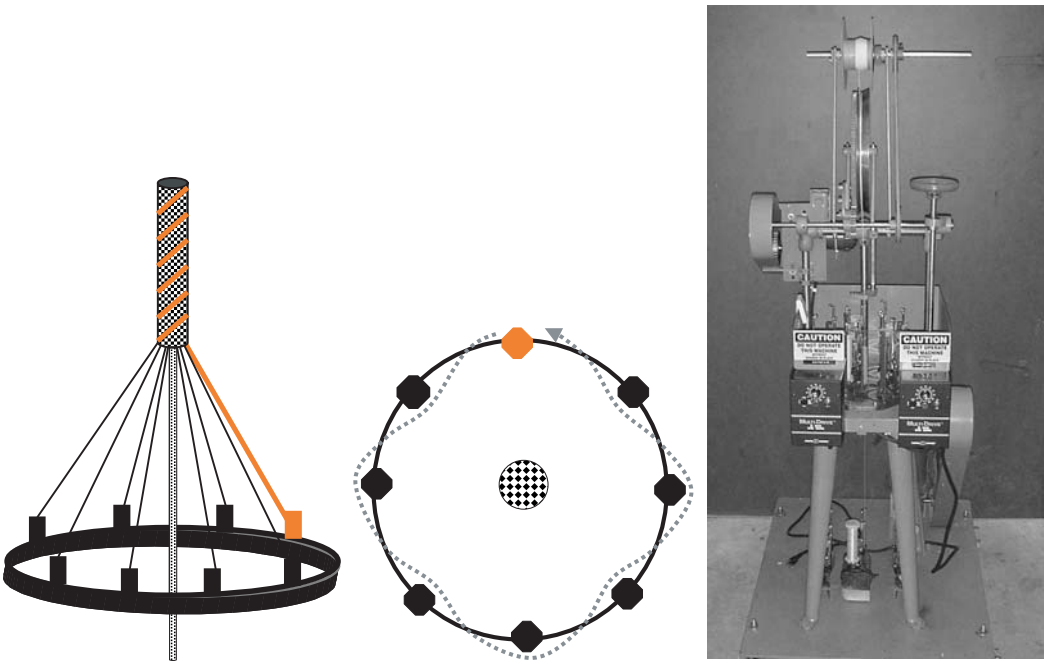

Figure 12.5 (Left) Schematic of tubular braiding machine. Fibers and wire (indicated in gray) are spooled from carriers that rotate on a circular track. Fibers may be braided around a center mandrel or other fibers in the core of the braid. (Center) Arrow indicates path taken by one yarn carrier in maypole braiding pattern. (Right) Photograph of tubular braiding machine at CEAM.

braid itself is a tough structure that protects elements woven into the outer sheath, as well as other elements in the core. Thus functional elements (wires and/or perhaps sensors) are truly integrated into the fibers of the host composite, rather than acting as inclusions in the matrix phase. Furthermore, braiding allows fine control of the pitch and diameter of the wire coil such that the electromagnetic properties may be tuned for desired performance. The sense of the coil, as left-handed or right-handed, may also be varied in this process to address issues of chirality, as discussed below (see Amirkhizi et al., 2003).

12.2.1.2.1 Chirality

The introduction of coil geometry not only affects the inductance of the medium and consequently the overall dielectric constant, but also introduces different capacitative response than mere straight wires. This capacitative response usually changes the overall magnetic properties of the medium, although the inductive response still remains the dominant effect. Part of the magnetic response is induced by the chirality effect which is discussed presently. However, a more careful and thorough study is needed since the techniques that can be used to eliminate chirality do not necessarily change the axial magnetic effects.

Of importance is the effect of the handedness of the coils on the EM field vectors. The geometry of the coils requires that the current density in the conductors has a circumferential component, in addition to the axial component which is the only component present in the case of the straight wires. The oscillating circumferential component of the current enhances the magnetic field of the propagating wave with a component parallel to the axis of the coils. Note that as the active component of the electric field is parallel to the axis of the coils, the accompanying magnetic field is normal to it. Therefore the enhanced magnetic field is normal to the external excitation.

Moreover the extra component is in phase with the current density and in turn with the external electric field, whereas the external magnetic field and electric field are out of phase by a quarter of a

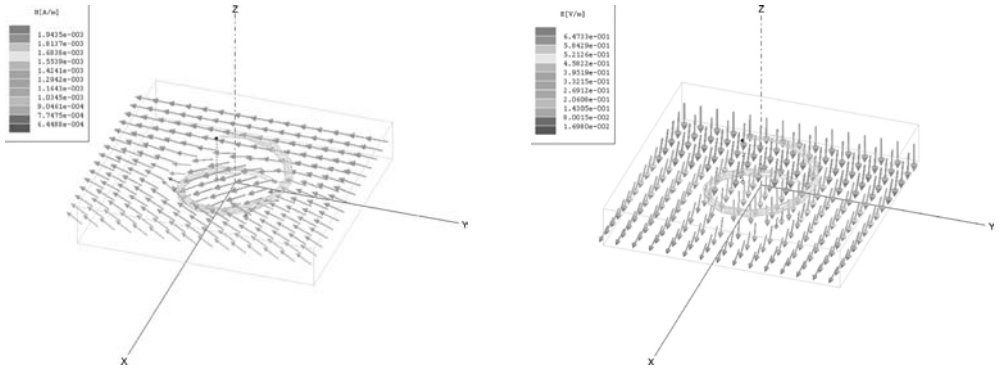

Figure 12.6 (See color insert following page 302) Electric field (left) and magnetic field (right) patterns calculated for a unit cell of a coiled medium using ANSOFT-HFSS. The wave is propagating in the *x*-direction and the fields on the two *yz* faces have 50° phase difference. The incoming wave (electric field) from the far *yz* face is at this time polarized parallel to the axis of the coil. However, the effect of the coil adds an out of phase normal component. Therefore, the field vectors of both electric and magnetic fields rotate as the wave travels through the cell.

cycle. If the created magnetic component were in phase with the external excitation, the superposed field would be slightly skewed from the original field. This would have meant that one could still define principal axes for the material property tensors, although they are slightly angled compared to the structural axes. However, the phase incompatibility creates rotating magnetic fields which in turn create rotating electric fields. The principal propagating polarizations are not linear any more, but rather have elliptical polarization (see Figure 12.6).

The effect of chirality can be used to benefit some applications. However, in most cases, it may introduce unwanted complexity. In order to eliminate this behavior, two methods have been proposed. The first method is to include alternating coils in the array so that every right-handed coil should be adjacent to a left-handed coil. We considered this solution only for regular arrays as will be discussed, but we conjecture that since the wavelength is much larger than the spacing between coils for effective media, a randomly homogenous and statistically equal distribution of the right and left-handed coils should also have a similar effect. Note that for an irregular medium, the size of the volume that is randomly homogeneous must be considerably smaller than the wavelength as compared with a regular array. Another way to eliminate the chirality effect is to use double coils instead of simple single coils. If two concentric coils with the opposite handedness are together, most of the magnetic field created by the circumferential electric current is effectively canceled.

In the first method, one can stack alternating layers of right- and left-handed coils together. The traveling wave undergoes the opposite effects of the two layers and therefore the polarization of the fields will not be rotated. Another arrangement that has the same effect is to design each layer to have alternating coils. In other words, instead of having alternating layers in the thickness direction, one has alternating layers in the normal direction. Moreover by shifting these layers by one lattice spacing, one can achieve a 2-D checker board design. These three designs have similar behavior and do not significantly affect the plasmon frequency, compared to the original chiral medium. The design with alternating layers normal to the propagation direction is preferable, since the period length in the propagation direction is smallest and therefore the diffraction frequency limit is higher, as shown in Figure 12.7.

In the second method, the effect of clockwise or counter-clockwise circumferential current is not cancelled by adjacent coils, but by a local and concentric coil of the opposite handedness. The attraction of this method lies in the fact that no special ordering or arrangement at the time of manufacturing of the composite is required. The double coils can either be made by a two-stage braiding scheme or a similar design can even be achieved by braiding the conducting coils of insulated wires at the same time in opposite orientations. The double coils may have an advantage

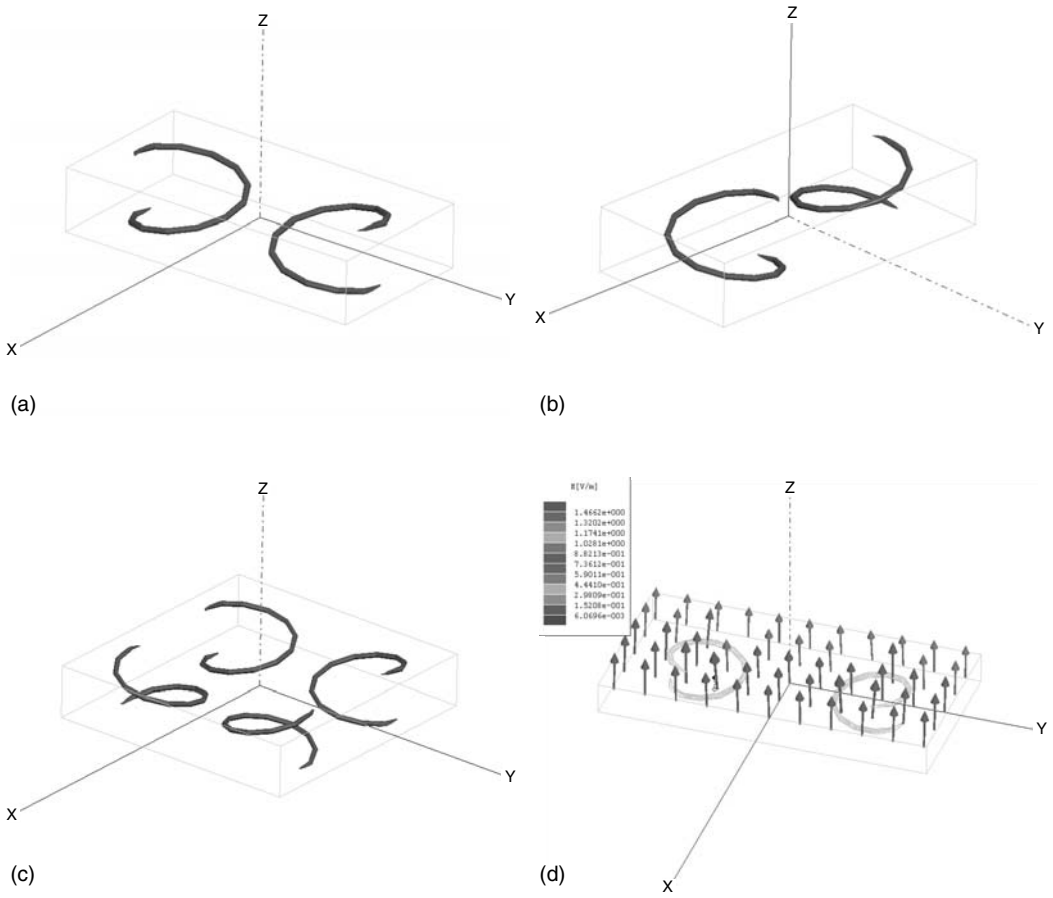

Figure 12.7 Alternating arrays of left-handed and right-handed coils. Considering an EM wave is propagating through the medium in the *x*-direction, each of the above sets can be used to cancel the polarization rotation effect. To envision the whole array, imagine these as blocks and fill the 3D space with similar blocks in each case (only translated by the size of the block in each direction). Top left: Each layer through the thickness consists of alternating coils. The layers are then stacked, such that normal to the thickness, the coils are similar. Top right: Layers of uniform right-handed and left-handed coils are stacked through the thickness. Bottom left: Checker board configuration. All four adjacent coils to any single one are of opposite handedness. Bottom right: The effect of the field rotation is canceled. However, the linear polarization of the electric field parallel to the axis of the coils is maintained through the medium. Note that the periodic length of the medium for the top right and bottom left cases is twice as much as it is for the top left case, hence providing a smaller diffraction frequency limit. The dispersion relation and plasmon frequency for the principal propagating modes remain essentially unaltered compared to the uniform arrays. However, the modes are dramatically different.

in mass production of composites. However, the additional inside loop increases the plasmon frequency and reduces the effective range of the pass band. Numerical studies show that higher pitch values can overcome this difficulty, as indicated in Figure 12.8. Simulation parameters for these results are given in Table 12.1.

12.2.1.3 Braided Composite Manufacturing

As an example, we have braided coil elements with para-aramid (DuPont Kevlar®) reinforcing fiber and polyamide (DuPont nylon 6,6) thermoplastic fiber. The outer braid consists of a single 30 gauge (0.254 mm diameter) copper wire, four ends of 200 denier Kevlar fiber, and three ends of 210

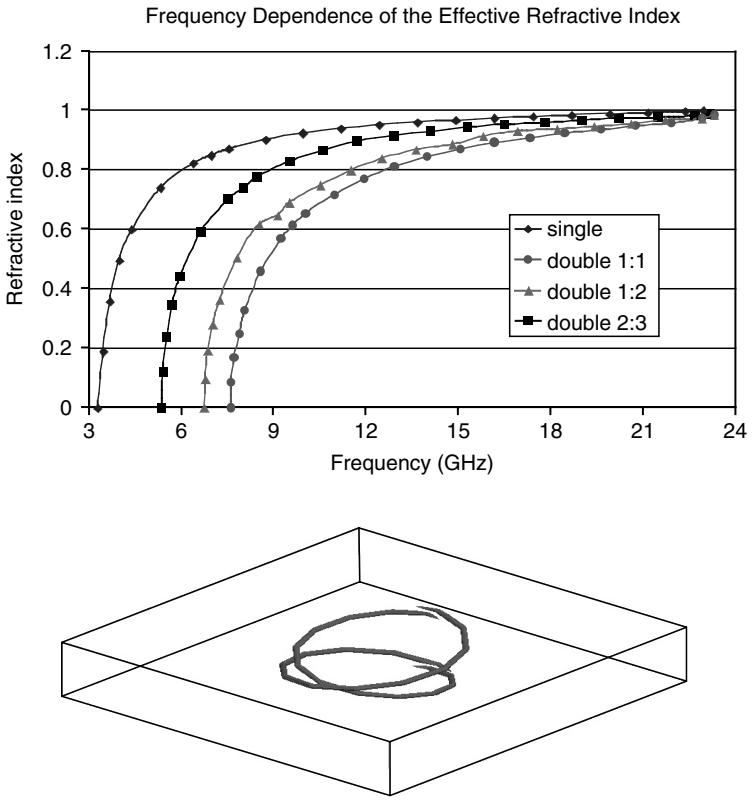

Figure 12.8 (Top) Frequency dependency of the effective refractive index for various coil geometries. Double coils (bottom) can also be used to cancel the effect of chirality. However, they also modify the plasma frequency of the medium as the effective inductance and capacitance per unit volume is changed.

denier nylon fiber. The core of the braid consists of one end of 1000 denier Kevlar fiber and three ends of 420 denier nylon fiber. An illustration is provided in Figure 12.9 showing the constituents of the braid architecture. Nylon is included in the braiding process since it will serve as the polymer matrix of the final composite, although it may not be the optimal choice in terms of mechanical strength of the resulting composite. Complete fiber wet-out can be a difficult processing challenge in braided composite materials, due to the inherent tight packing of fibers in the braiding process. We have initially addressed this issue by developing a commingled braid composite, which integrates the eventual matrix phase as a thermoplastic fiber that is braided along with the structural

Table 12.1 Parameters for Simulating Various Coil Geometries in HFSS Electromagnetic Simulations

		Single	Double 1:1	Double 1:2	Double 2:3
Outer cell	Spacing (mm)	6.35	6.35	6.35	6.35
	Cell height (mm)	1.1	1.1	1.1	1.1
	Inner diameter (mm)	2.6	2.6	2.6	2.6
Inner cell	Turns in one cell	1	1	2	3
	Inner diameter (mm)	—	2.2	2.2	2.2
	Turns in one cell	—	1	1	1
	Wire thickness (mm)	0.1	0.1	0.1	0.1
	Plasma frequency (GHz)	3.26	7.59	6.73	5.35

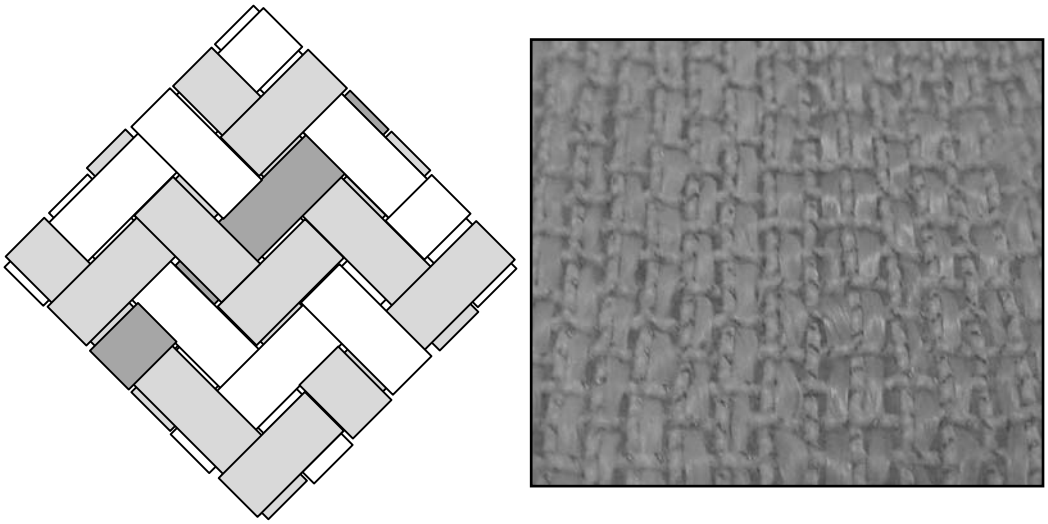

Figure 12.9 (Left) Schematic of outer braided architecture with 2 up 2 down braid pattern consisting of Kevlar fibers (light gray), nylon fibers (white) and copper wire (dark gray). (Right) Photograph of braids bi-directionally woven into fabric with additional Kevlar fibers. Coils with opposite sense are woven adjacent to one another.

fibers. Overall, the composite is designed to have a Kevlar fiber volume fraction of about 50%. Selection of the diameter of the core allows control of the diameter of the coil that is braided around it. The core may be composed of various other elements, including other electromagnetic elements, or perhaps sensors, though in this initial design we have incorporated only reinforcing fibers. The pitch of the braids is determined by the take-up and rotation speed of the carriers. The pitch of these coils was maintained at 60° from the axis of the braid.

The braided elements take the form of a laminate by weaving with other reinforcing fibers to form a cohesive fabric. The braids may be oriented in a single direction in each layer or may be woven together bi-directionally. Due to the inherent stiffness of the dry braid, tight weaving patterns in a bi-directional weave, such as plain weave and satin weave, may be restricted since the braid cannot be woven over small intervals without kinking, which compromises the braid structure. This factor is dependent on the braid and wire diameter, where smaller diameters are not subject to such limitations. This limitation is avoided when braids are woven uni-directionally since the fill yarns (weft direction) are able to accommodate such undulation while allowing the braid elements (warp direction) to remain straight. To achieve the desired spacing of the coil array, while maintaining a uniform composite fabric, blank braids may be woven into the layer or inserted between layers. The blank braid is identical to the electromagnetic braid element, however, the copper wire is replaced with an end of reinforcing fiber. Additionally, as mentioned above, chiral effects of the coil geometry can be eliminated by alternate placement of a left-handed coil next to a right-handed coil. Such an arrangement can be easily achieved in the braiding and weaving processes. Woven layers are stacked in accord with the electromagnetic design and processed with additional thermoplastic matrix at elevated temperature and pressure to form the consolidated composite.

These braided elements have been integrated into a composite panel and characterized electromagnetically. Figure 12.10 shows such a panel consisting of Kevlar braids woven into laminates and pressed into a nylon matrix composite. The coils were arranged in an alternating square matrix in one direction of the composite. Hence, the panel showed a plasmon response in one orientation and not in the other. The experimental results showed good agreement with our simulations. The dielectric constant of the structure is measured as a function of frequency

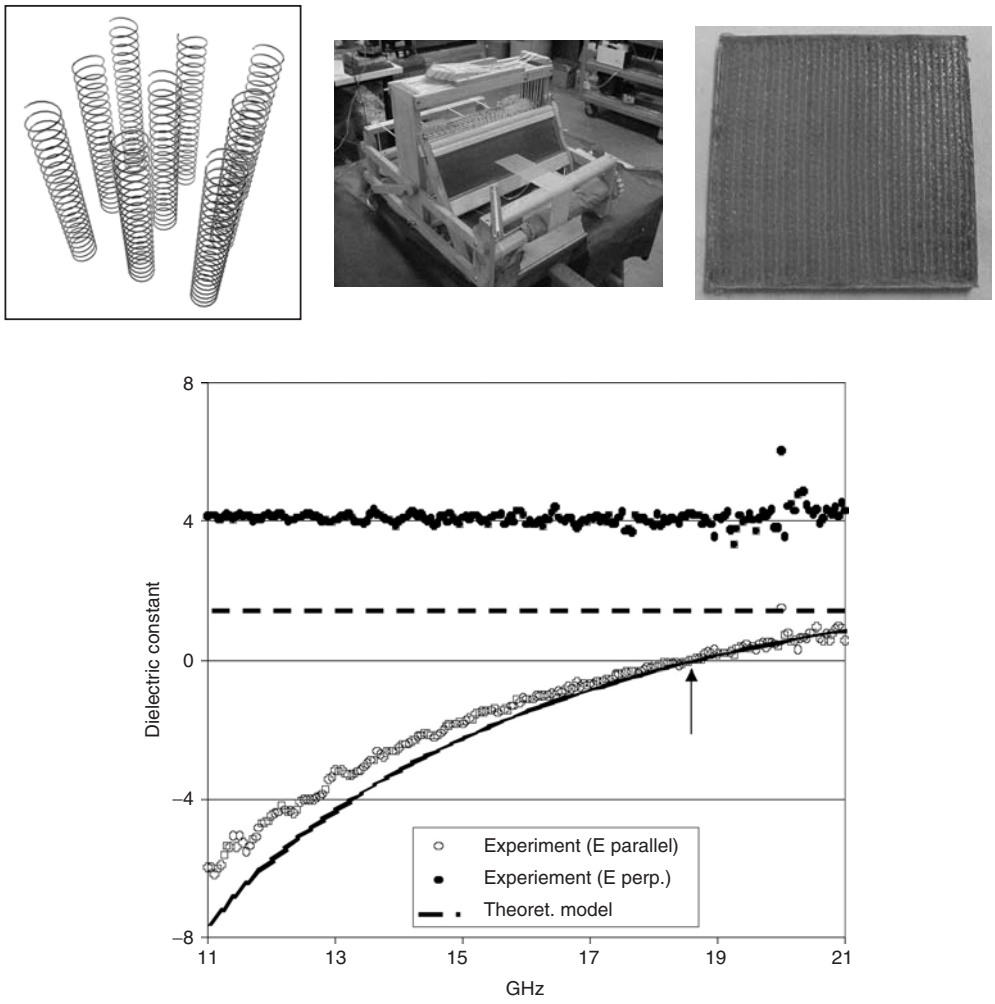

Figure 12.10 (See color insert following page 302) (Top) Coiled wire architecture integrated with structural Kevlar fibers by braiding. Braids woven and laminated into composite plates. (Bottom)EM characterization of the braided or woven composite showing typical plasmon media response when aligned parallel to the polarization of the EM radiation. Normal (nonplasma) dielectric response is observed when aligned in the perpendicular direction.

from 11 to 21 GHz, whereupon at around 18 GHz, the dielectric constant passes through zero. This dispersion relation follows the characteristic trend of the thin straight wire arrays studied previously. Between the plasma frequency and the upper limit of our frequency sweep, the dielectric constant of the composite array approaches unity. Since the index of refraction of the material is the square of the dielectric constant, we may also conclude that the index approaches unity.

12.2.1.4 Controlling the Effective Magnetic Permeability

Following Pendry et al. (1999), Smith et al. (2000a,b), and Shelby et al. (2001), we have shown that the effective magnetic permeability, μ, of free space can be rendered negative over a certain frequency range by suitably integrating the so called split-ring-resonators, as shown in Figure 12.11. The structure, however, cannot be integrated into a thin composite panel. To remedy this fundamental barrier, we considered collapsing the rings into nested folded plates, as shown in

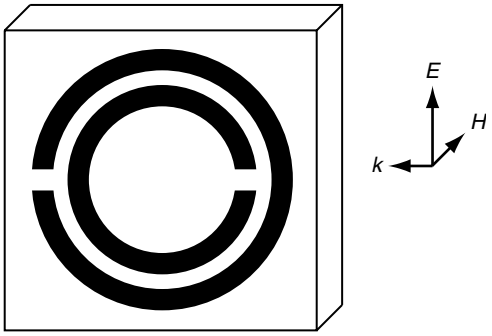

Figure 12.11 Original SRR design with wave vector *k*, electric *E*, and magnetic *H* fields indicated for effective negative permeability.

Figure 12.12, and called the construction folded-doubled-resonator (FDR). Measurements, using a focused beam EM characterization system, Figure 12.13, revealed that indeed the composite had a negative μ over a frequency range of about 8.5 to 9.5 GHz. Following this, a new design was conceived, numerically simulated, and constructed that had a more pronounced negative μ. This construction is shown in Figure 12.14, and the measured results are given in Figure 12.15. As is discussed in the next section, combining the negative ε and μ, it is possible to construct a composite panel with negative index of refraction.

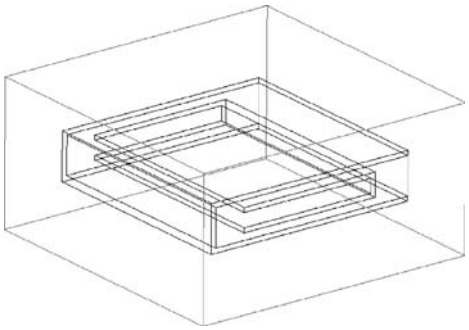

Figure 12.12 FDR design produces the required resonance with a thickness that lends itself to inclusion into an actual composite panel of reasonable thickness.

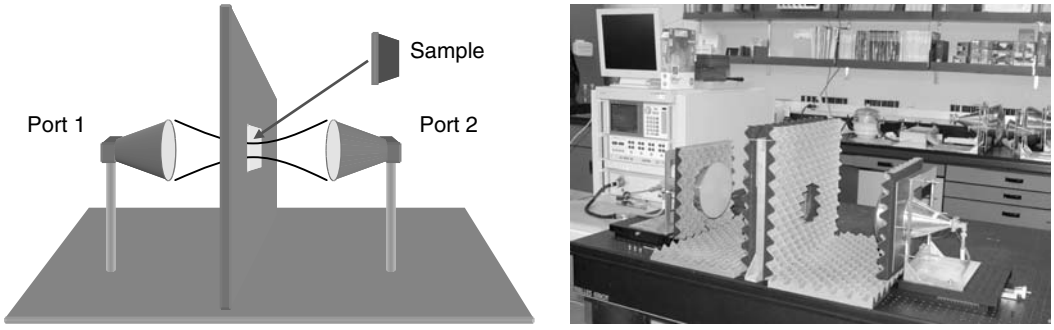

Figure 12.13 (See color insert following page 302) (Left) Schematic and (right) photo of Focused Beam system for EM characterization from 5 to 40 GHz at UCSD's CEAM.

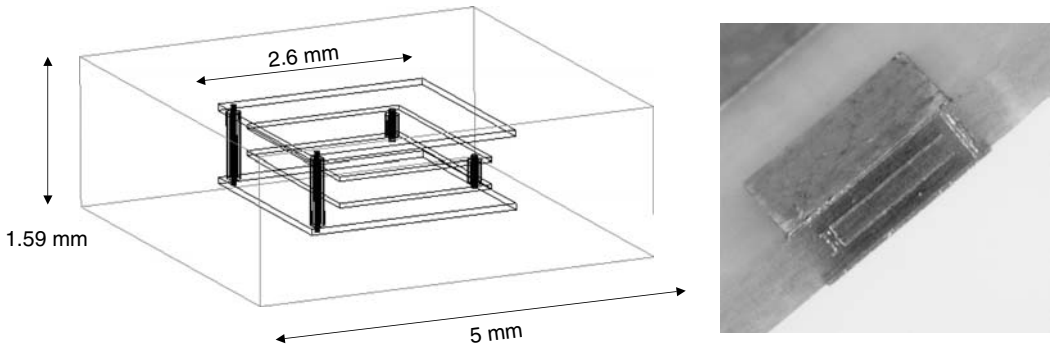

Figure 12.14 FDR unit cell and dimensions (left); and fabrication within a composite panel (right).

12.2.1.5 Negative Refractive Index Composites

As mentioned above, over the past several years, the authors at UCSD's Center of Excellence for Advanced Materials (CEAM) have developed methods to design, fabricate, and characterize NIMs, and have demonstrated these capabilities in illustrative microwave experiments. Composite panels of 2.7 mm thickness have been produced that possess through-the-thickness negative index that has been measured unambiguously by full S-parameters retrieval, as discussed below (Starr et al., 2004). Such samples are relatively easy to characterize, as both transmission and reflection measurements can be carried out on very thin samples.

Several views of the actual panel along with the dimensions of the elements within a unit cell of the CEAM NIM are shown in Figure 12.16–Figure 12.18. The elements that give rise to both electric and magnetic response are fabricated using multi-circuit board techniques. The composite is assembled from three laminated layers. The top and bottom layers consist of Rogers 4003 circuit board laminates ($\varepsilon = 3.38$, tan $\delta = 0.003$), with a prepreg layer of Gore SpeedBoard ($\varepsilon = 2.56$, tan $\delta = 0.004$). The measured (solid) and simulated (dashed) values of the real (black) and imaginary (gray) index of refraction are shown in Figure 12.19.

The layers are bound together by a layer of adhesive at the interfaces between the Gore and Rogers circuit boards. Both of the Rogers circuit boards initially have a thin layer of copper (half-ounce or approximately 1 μm in thickness) deposited on both sides from which the elements are patterned using conventional optical lithography. The wire elements are patterned on the sides of the Rogers boards that face the Gore SpeedBoard. This prototype was manufactured by Hughes Circuits.[2]

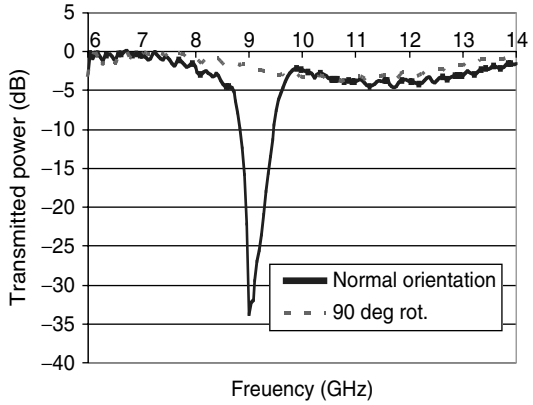

Figure 12.15 Negative magnetic permeability experimentally demonstrated from about 8.5 to 9.5 GHz for the FDR structure.

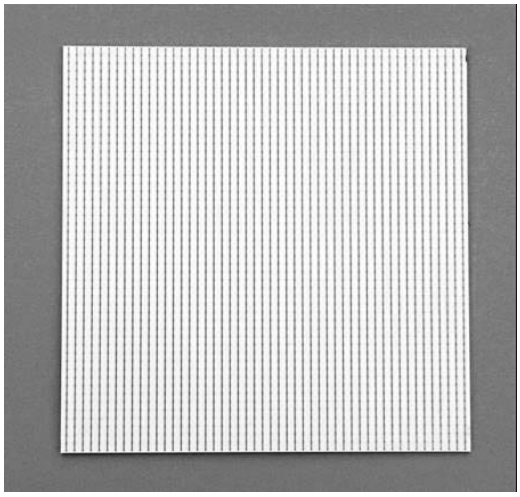

Figure 12.16 Planar view of the CEAM NIM.

12.2.2 Heating Functionality

Initial simulation and testing has been conducted to demonstrate the heating capabilities of our integrated thin wire arrays (Plaisted et al., 2003a,b; Santos et al., 2004). Using the same wire diameter and array dimensions as designed for EM functionality, we have applied direct current to resistively heat a composite sample. Embedded wires are currently used for resistive heating as a method of welding thermoplastic polymers and polymer composites (Eveno and Gillespie 1988; Jakobsen et al., 1989; Ageorges et al., 2000) Similarly, embedded heating elements have been used to cure the resin matrix in thermoset polymer composites (Sancaktar et al., 1993; Ramakrishnan et al., 2000).

12.2.2.1 Simulation and Testing

The thin copper wires in our composite can be connected to a DC electrical source and leveraged as heating elements, dissipating heat as a result of Ohm's Law:

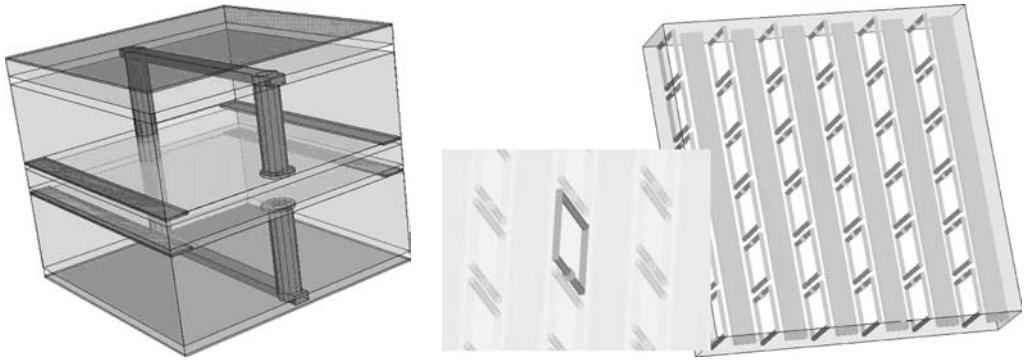

Figure 12.17 (See color insert) (Left) Unit cell of NIM. The negative permeability is achieved by ring resonators, formed from copper strips on the upper and lower surfaces, connected to vias that run through the structure, with one of the vias possessing a gap in the center to introduce capacitance. Copper strips are patterned on the central circuit board, giving rise to the negative permittivity of the structure. (Right) Views of conducting elements as they are fabricated within a composite panel.

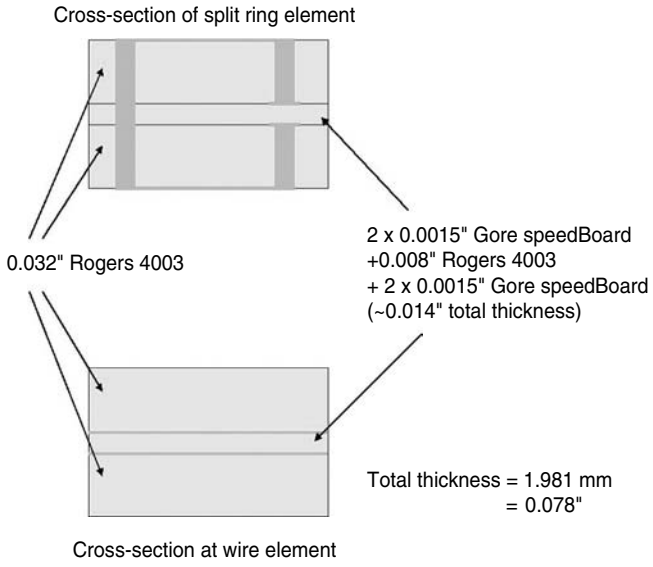

Figure 12.18 Dimensions for cross-sectioned view of NIM.

$$P = VI = I^2R = V^2/R \tag{12.3}$$

where P is power, V is voltage across the circuit element, I is direct current through the circuit, and R is the resistance of the circuit element. Finite element computer simulation software, NISA, is used to model the heating in conjunction with experimental testing. The heat transfer module of NISA, known as NISA/HEAT, uses finite element methods to solve the heat conduction equation for temperature based on a set of initial and boundary conditions.

Our thin wire arrayed composites typically have a spacing of 0.125 in. (3.175 mm) between copper wires of 100 μm diameter. To simulate this geometry in NISA's graphical interface, a unit cell of 0.125 in. by 0.125 in. is constructed to represent a cross-section of the composite as shown in Figure 12.20. To reduce calculations to a 2-D problem, the unit cell is assumed to have unit depth and a constant cross-section along the length of the wire.

A square element mesh is applied to the unit cell, with the circular cross-section of wire approximated by a square pattern of four elements. Boundary conditions are prescribed on the

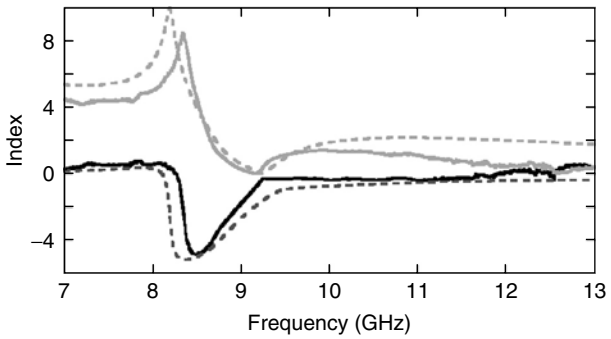

Figure 12.19 Recovered refractive index (n) from simulation data (dashed curves) and from measured S-parameters (solid curves). Black and gray curves represent the real and imaginary parts of the refractive index, respectively.

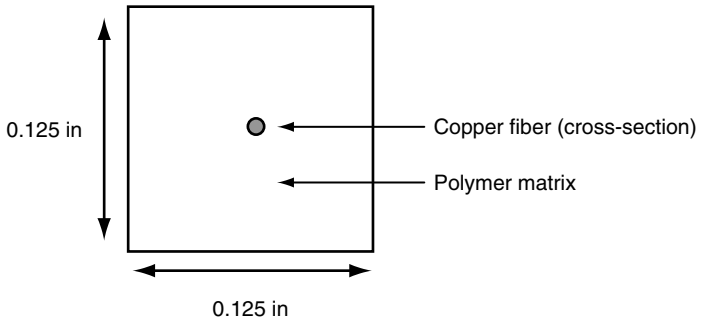

Figure 12.20 Unit cell geometry for NISA simulation of resistive heating scheme.

mesh based on: thermal conductivity, mass, density, and specific heat of the material; electrical power input and heat generation; and conditions at the edges of the unit cell. We approximate the thermal properties of the polymer matrix with those of epoxy commonly used in composites. These properties are prescribed on the polymer elements of the mesh, while the properties of annealed copper are prescribed on the wire elements. It is assumed that the electrical power input is constant over time and converted fully into heat, so a constant heat generation is prescribed on the wire elements. The conditions at the edges of the unit cell are either "insulated," implying that boundaries of zero heat flux are prescribed on all edges of the cell, or "exposed to air," where convection boundary conditions are prescribed on two opposite edges of the cell instead of zero heat flux. The insulated condition simulates a unit cell surrounded on all sides by identical material through periodic boundary conditions.

According to the results of our simulation, the temperature of the insulated unit cell increases linearly for a constant power input, while the temperature of the exposed unit cell holds constant after a period of time (Figure 12.21). Also, the temperatures at different locations in the exposed unit cell vary by as much as 15°C, as shown by the multiple lines on the graph. For the insulated unit cell, the temperature distribution differs by 4°C at the most. The power density value (W/cm^2) in these graphs denotes power distribution over the flat area of the composite panel, *not* the power distribution over the cross-section.

A sample composite panel was fabricated from glass–fiber-reinforced epoxy prepreg and 100-μm copper wire to test the resistive heating process. Copper wires were strung in a parallel arrangement in one direction and three thermocouple wires were included at various depths between the prepreg layers to monitor internal temperatures. The dimensions of the panel were

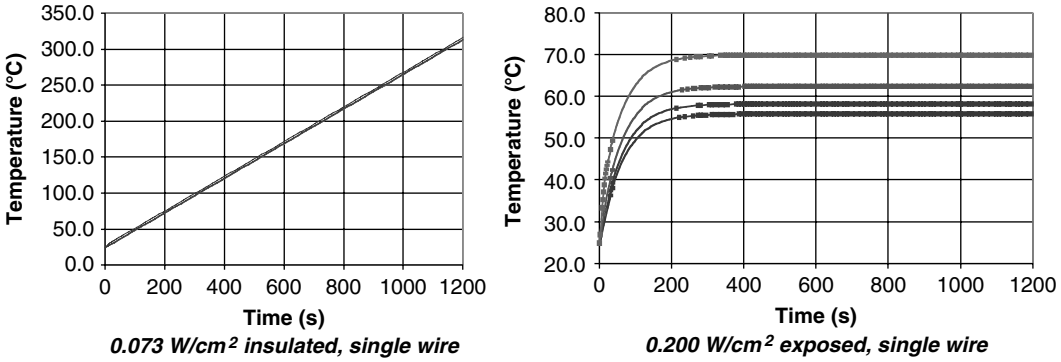

Figure 12.21 Simulated temperature vs. time response for insulated (left) and exposed (right) unit cells. Multiple lines indicate temperatures at various locations within the panel.

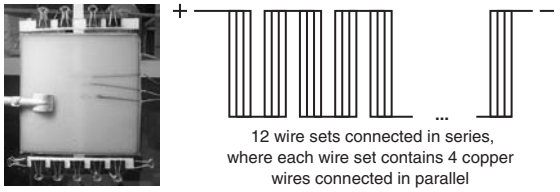

Figure 12.22 (Left) Composite panel in conductor frame. Embedded thermocouple wires protrude to the right of the panel. (Right) Abbreviated circuit diagram.

15 cm by 15 cm by 0.32 cm thick and its fiber volume fraction was around 60%. After curing, the copper wire strands that protruded from the edges of the panel were retained since they provided electrical connection.

The wires in the composite panel were combined into a single circuit by a custom apparatus we refer to as a conductor frame. The frame consists of conductor bars to which adhesive copper strips are attached. By clamping groups of wires to the conductor bars, a combined series–parallel circuit through the entire panel is created (Figure 12.22). The copper strips extend around the sides of the upper conductor bar so that they may be connected to the power source. The DC power source used in these tests was a voltage generator with maximum output of 36 V and 8 A. In addition, the thermocouple wires were connected to a multi-channel thermocouple monitor. To measure the electrical power input, two multimeters were included in the setup to measure total voltage across all wires in the composite and total current across the entire circuit.

The voltage for our initial tests was based on simulation and remained constant throughout each individual test. The voltage was then iteratively optimized in subsequent tests to achieve our target temperature. Prior to turning on the power source the initial temperature for all thermocouple channels was recorded. Once power was supplied to the composite panel, temperatures were recorded for each of the thermocouple wires at 30-s intervals. The voltage and current were also recorded every 30 seconds for a total duration of about 20 min.

Noninsulated test conditions were conducted with the panel configuration as shown in Figure 12.22. To test insulated conditions, sheets of cotton-like fiberglass were placed on both sides of the panel to minimize heat loss. The results of the resistive heating tests are qualitatively similar to the results of the finite element simulations. The temperature for an insulated composite rises almost linearly, while the temperature in the exposed composite rises quickly at first before holding constant (Figure 12.23). However, the quantitative results differ noticeably between simulation and experiment. For insulated conditions, the temperature after 1200 s is above 300°C in simulation, whereas the temperature in the actual test only exceeds 80°C. This error is less pronounced for the exposed case; the simulation predicts a maximum constant temperature of 70°C while the test results have a maximum temperature of 84°C. However, the simulation of exposed conditions

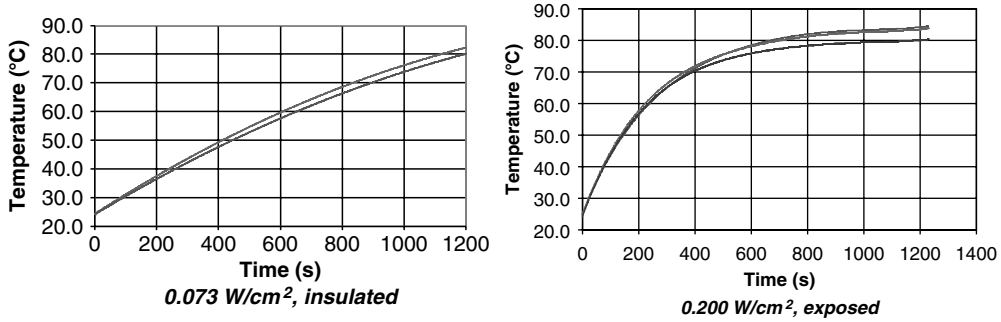

Figure 12.23 Experimental temperature vs. time for insulated (left) and exposed (right) panels.

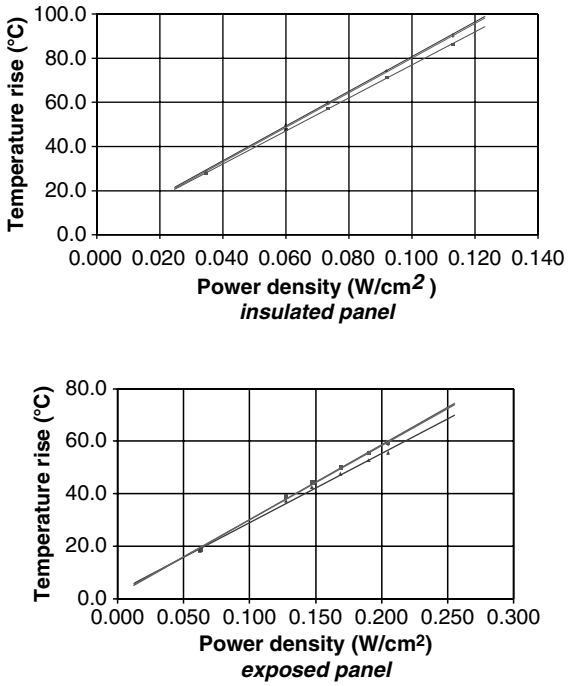

Figure 12.24 Experimental temperature rise vs. power density for insulated (left) and exposed (right) panels.

predicts a local temperature difference of 15°C between different areas in the composite, while this temperature difference is only about 5°C in the actual test.

The tests were carried out for different levels of electrical power, and a linear correlation was found between the final temperature and the power input (Figure 12.24). Power density over the face of the panel is used in place of total electrical power so that the value is normalized for any size of composite panel. Temperature rise is used in place of the actual final temperature so that temperature results are normalized for any initial temperature. According to the graphs, an insulated panel requires about 60% less power than the exposed panel to reach the same temperature. If an ambient temperature of 20°C is assumed, and our target temperature is 80°C, then a temperature increase of 60°C is desired, which corresponds to 0.073 W/cm^2 power input for the insulated panel, compared to the exposed panel's 0.20 W/cm^2.

Thermal management within the composite may be leveraged for a number of applications. In our multifunctional composite, we may utilize this heating function to induce a thermally activated healing process as detailed in the next section.

12.2.3 Healing Functionality

A material that can heal itself is of great utility where access for manual repair is limited or impossible, as in a biological implant or a material that is launched into orbit in the solar system. Structures made of such a material may have significantly prolonged service life in addition to improved safety if failure mechanisms such as cracking can be repaired *in situ*. Nature has long demonstrated this property in various biological materials, whereas, until recently, man-made healing materials have essentially not been demonstrated. However, interest in synthetic healing materials has recently gained significant attention with the creation of a truly autonomic healing polymer by White and other researchers at the University of Illinois (White et al., 2001). Since then other healing materials have been proposed (Bleay et al., 2001; Chen et al., 2002), one of which is a novel polymer that will be the focus of further research at UCSD. Wudl and his research group at

UCLA have created a strong, tough polymer that forms a high degree of thermally reversible, covalent cross-links. Mechanical failure of this polymer occurs preferentially along these cross-links, and due to the reversible nature of this bond it may be repaired by application of moderate pressure and heat.

12.2.3.1 Polymer Healing

Polymers offer many attributes that allow for healing of damage within the material. Polymers consist of long chain molecules with molecular weights ranging from 10^4 to 10^6. These long chains are made up of a string of monomers, which are the molecular repeat unit identifying that particular polymer. Linear, branched, and the other nonnetworked polymers generally form amorphous or semicrystalline polymers with thermoplastic character. Interaction between chains occurs through noncovalent bonding such as hydrogen bonding and chain entanglements. As a thermoplastic, the polymer may be heated to its melting temperature and solidified repeatedly with little change in the properties. In contrast, thermosets consist of cross-linked networks formed by covalent bonding and will degrade, rather than melt, upon heating.

Healing damage within a polymer is most often associated with the softening and flow of material across a damaged interface that occurs upon heating a thermoplastic polymer. This technique is commonly known as thermoplastic welding. Healing in thermoplastic polymers occurs largely due to the restoration of entanglements in the polymer interface. Secondary bonding between chains, in the form of van der Waals or London dispersion forces, is also critical to the healing process. Other bonding, such as hydrogen bonding and chemisorption, can play an important role. Chains are able to diffuse across the interface when heated above the glass transition temperature, T_g. The rate of crack healing is strongly time dependent, as the once separated molecular structures diffuse across the interface to form an equivalent bonding state to that of the virgin material. Crack healing in thermoplastic polymer surfaces seldom results from the reformation of broken bonds (primary bonds) in the polymer backbone. Typically the polymer chains at the crack interface have been irreversibly damaged through bond breakage which results in an average molecular weight significantly lower than that of the bulk polymer. Furthermore, the catalyst for polymerization (through addition or condensation reactions) is not present to repolymerize the material. The crack healing and welding in thermoplastics has been widely studied in the literature, particularly by Wool and Kausch and their co-workers (Wool, 1978, 1979, 1995; Jud and Kausch, 1979; Jud et al., 1981; Wool and O'Connor, 1981a,b, 1982; Kausch and Jud, 1982; Kausch, 1983; Kausch et al., 1987; Kausch and Tirrell, 1989; Wool et al., 1989)

Healing damage within thermoset polymers is typically not possible due to the cross-linked nature of these materials. The cross-link network prevents the polymer chains from diffusing through the material when heated above the T_g. Rather the material begins to thermally degrade when heated excessively, and in contrast to thermoplastics, cannot be returned to its original state. Until recently, there has been no evidence of repairing damage in highly cross-linked materials. An interesting repair scheme has been proposed by White et al. to embed a healing system within an epoxy polymer (White et al., 2001) Liquid monomer is microencapsulated and embedded with dispersed catalyst in an epoxy polymer, such that a propagating crack intersects a microcapsule and releases the healing agent to effectively glue the crack shut. A schematic of the healing process is given in Figure 12.25. Another system, proposed by Wudl and coworkers, uses a novel reversible bonding approach to repair cross-links (Chen et al., 2002). It is this polymer that has been utilized in the multifunctional material under development at UCSD.

12.2.3.2 Thermo-Reversibly Cross-Linked Polymer

In 2002, Wudl and coworkers published work on a polymer with the ability to repair internal cracking (Chen et al., 2002). Until that time, there had been no highly cross-linked polymers that

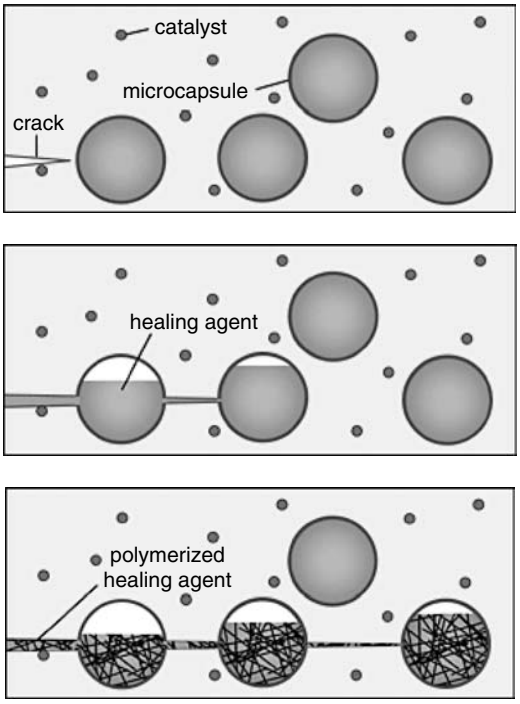

Figure 12.25 Healing concept of an autonomic healing polymer (White et al., 2001).

could be repaired without the use of additional monomers or surface treatment to repair a cracked interface. Chen et al. accomplished this by synthesizing a polymer based on a thermally reversible Diels–Alder (DA) and retro-DA cycloaddition. The Diels–Alder cycloaddition is a widely used reaction in organic synthesis. Many polymers involving the DA cycloaddition have been synthesized, though in many cases the retro-DA reaction is not observed if the diene and dieneophile are not sufficiently stable on their own. Those polymers with suitable monomer combinations to exhibit the retro-DA reaction have incorporated the DA adduct into the backbone of the polymer (Chujo et al., 1990; Engle and Wagener, 1993; Imai et al., 2000) In contrast, the unique aspect of the polymer created by Chen et al. is that all of the monomer linkages, or cross-links, are formed by DA cycloaddition and furthermore exhibit the retro-DA reaction.

12.2.3.3 Healing Experiments

The weakest bond in the polymer structure is the polymerization or cross-linking bond of the DA adduct. While strong in comparison to other types of noncovalent chemical bonds, this is the first bond to break when the material is loaded to failure or heated above its transition temperature. However, because this bond is reversible, this is also the bond that reforms when the material is cooled below the transition temperature. To test the healing ability of this bond, quantitative testing of the fracture toughness was performed (Chen et al., 2003). Compact tension samples were notched with a razor blade and loaded in a direction perpendicular to the pre-crack. To arrest crack propagation in these tests, a hole was drilled into the middle of the specimen. In this way the cracks were arrested before fracturing the material into two halves and allowed more accurate alignment of the fracture surfaces during the healing treatment. Healing was carried out at 115°C for about 30 min with pressure applied by a clamp. Averaging over three tests, the material was able to recover 81% of its original fracture load. Furthermore, when the same healing procedure was applied a second time,

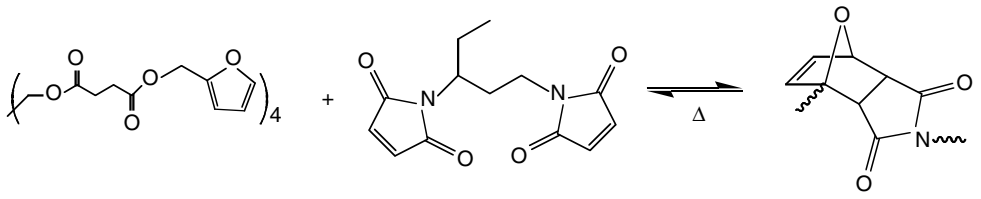

Figure 12.26 The polymer consists of a multifuran molecule combined in stoichiometric ratio with a multi-maleimide molecule.

the material recovered an average of 78% of the original fracture load, indicating that the material could be repaired multiple times. It was noted that the crack usually propagated along the same crack plane.

In addition, we have observed the healing mechanism in samples of this healable polymer. Our aim was to arrest crack growth prior to complete fracture of the sample. In this way we could improve the ability to match the severed interfaces back to their original location prior to heating. Due to the inherent high mechanical strength of this material, a controlled cracking procedure was devised. Samples were machined to 0.25 in. by 0.15 in. by 0.20 in. dimensions with a 0.08 in. diameter hole penetrating through the middle. Two notches were cut into the hole to initiate the crack on opposing sides of the hole. The samples were cooled in liquid nitrogen and immediately loaded in compression in the direction of the machined notch. The applied load caused cracks to grow from the notches in a controlled manner in the direction of the applied load. Cracked samples were then placed in a spring device that applied compression normal to the crack faces so as to put the crack faces in contact. Heat was then applied at various levels and durations. For samples treated for at least 6 h above 80°C under a nitrogen atmosphere with about 8 kPa of compression normal to the interface, the crack was observed to disappear, indicating healing. In these cases, no visible scar remained, apart from the initial starter notch. These tests were only qualitative in nature. However, it appeared that the crack had been completely repaired and visually the material had been restored to its original state. Figure 12.27 shows representative photographs before and after the healing event.

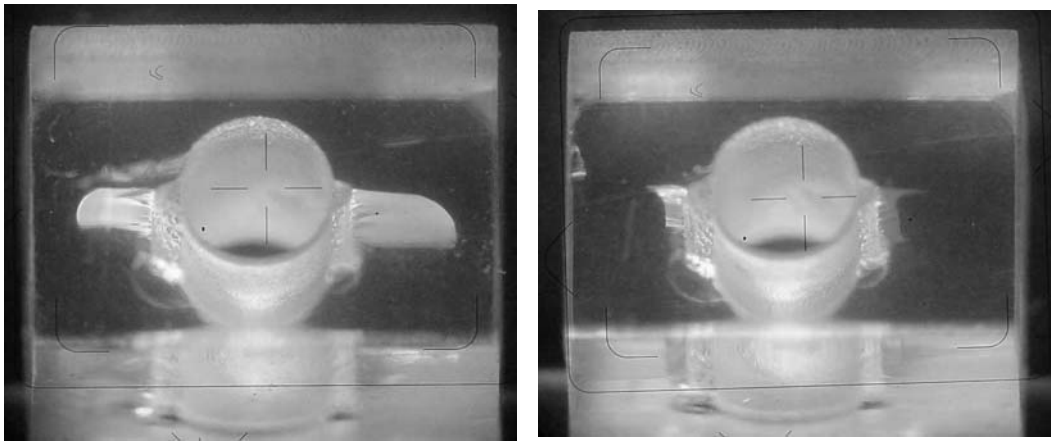

Figure 12.27 Optical photographs taken at 20 × magnification of representative healable polymer sample. Diagonal view of sample with predrilled hole and starter notches is shown. (Left) Polymer sample after controlled cracking. Note cracks have propagated from the starter notches to the left and right of the sample. (Right) Same sample after healing for 6 h under nitrogen and about 8 kPa of compression normal to the crack face. Crack faces have disappeared leaving only starter notches and predrilled hole visible.

12.2.3.4 Healing Summary

A cross-linked polymer with thermally reversible covalent bonds, such as that created by Wudl et al., offers many attractive attributes. When combined with a medium that distributes heat, such as a network of resistive heating wires, the healing mechanism may be initiated throughout the material. The effectiveness of such a system has yet to be fully determined, however, since healing occurs on the molecular level to reestablish broken covalent bond, there is considerable promise. Initial results on macro-cracked neat polymer samples show excellent potential that near full recovery of original strength is possible. Moreover, healing may be carried out multiple times on the same broken bond. This polymer requires outside intervention to initiate the heating (healing) process. We are developing self-sensing smart materials to embed in this material, where an integrated self-sensing, self-healing composite may act autonomously.

12.2.4 Sensing Functionality

The goal is to add *information-based* properties into multifunctional composites, mimicking nature's approach to local and global information acquisition, processing, and communication. Figure 12.28 identifies the necessary three interwoven challenges that must be successfully met in order to create intelligently sensing composite materials that are:

- Aware of their environmental and internal changes; and
- Can selectively acquire, process, and store or communicate information locally and globally.

As is suggested in this figure, integrating sensing functionality into structural materials begins with the challenge of composite fabrication that seamlessly integrates within the material the necessary sensing and electronic platforms, without sacrificing the structural attributes of the resulting system. The next challenge is that the structurally integrated micro-sensors must be able to monitor, interact with their neighboring sensors, make on-board decisions, and report on the local structural environment upon request, or in real-time as necessary. And, the final but equally vital challenge is to create an efficient data handling architecture with local–global processing and communication algorithms.

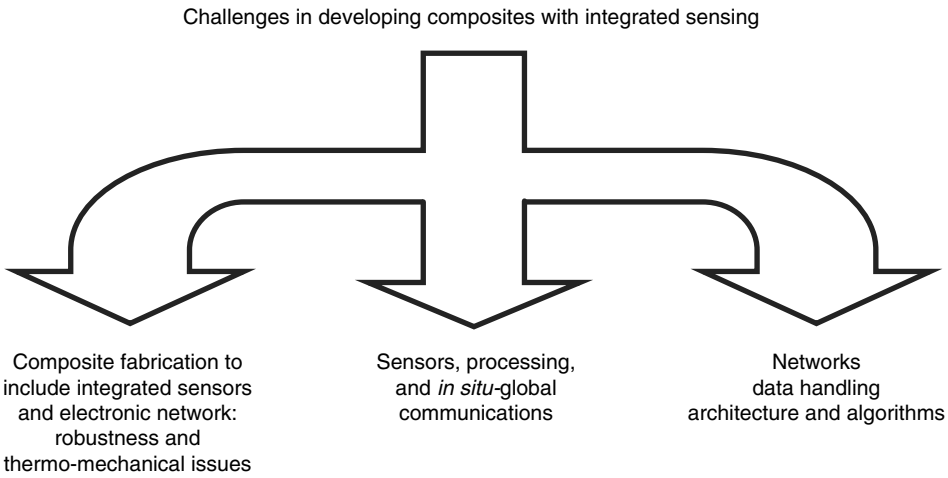

Figure 12.28 Three interwoven challenges that must be successfully met in order to create intelligently sensing composite materials.

12.2.4.1 Integrating Sensing into Composites

Here we focus on the development of a new type of composite with integrated high density of small, advanced sensors that would enable sensing without compromising the structural integrity. The volume of work in related areas is vast, and there have been a number of contributions aimed at incorporating novel nonstructural elements into composite systems (Varadan and Varadan, 2000; Lin and Fu-Kuo, 2002; Zhou and Sim, 2002). In this section we discuss several of the challenges associated with sensorized composites, including electronics, mechanical integration, and data management. We conclude by presenting results of some preliminary work.

12.2.4.2 Sensor Communications and Power

We seek to take advantage of advances in microelectronics, new capabilities in MEMS and sensor development, data feature extraction algorithms, multi-drop networking protocols, and composite fabrication technology to enable *in situ* sensing and damage detection at scalable, and potentially high areal density. Data bandwidth limitations require local data handling and efficient processing algorithms. Power management will be necessary to make high sensor densities possible. Embedded sensors require both power and a means of communication. Ideally, this would be done with the fewest number of conductors possible, and use a multi-drop network if feasible. The 1-Wire® network allows for distribution of power and two-way communications among many devices over a single pair of conductors.[3]

The 1-Wire network is specified for operation over a supply voltage range of 2.8 to 6 VDC. The positive, or data, line is held high by a nominal 5 kΩ impedance source. Multiple devices may be attached to the same network wire pair. Each device has a unique 64-bit address. The network protocol uses half duplex communications in master–slave architecture, where devices respond only upon command from the master. The protocol uses serial bit communications at 16.3 kbps. An overdrive mode is available that increases the data rate to 142 kbps. The network protocol not only allows individual device addressing, but also enables a novel search algorithm that allows a network master to discover all unique 64-bit addresses on any particular network. Power is drawn by the network device from the data line while it is high, and stored onboard the device in a nominal 800 pF capacitor for use during the intervals when the line is low.

The presence of multiple devices on a single network can increase the capacitive load on the network. Reflections at longer network distances and higher capacitance per unit length conductor pairs can cause slew rate problems, and contribute to limitations in the total fanout, or number devices that can be accommodated on a single network. Active pull-up drivers, careful attention to line termination, and proper transmission line design can compensate some of these effects. A well-designed system might accommodate several hundred devices, and has been demonstrated in a laboratory setting (Dallas, 2004).

12.2.4.3 Mechanical Integration

Previous efforts to integrate sensors and MEMS devices into fiber-reinforced composites have often required that such a device be placed between the fiber layers of a composite as it is being fabricated. As a result, the device is usually surrounded by the matrix phase, typically a polymer, which is generally the weak phase within the composite. Interlaminar regions are often the source of failure within a composite due to delamination, since often there is no reinforcement in the thickness direction (this problem may be minimized by through-the-thickness stitching). Depending on the size of an embedded device, this region is further weakened by the presence of sensors which can serve as stress concentrators. These sensors act as discontinuities in transferring stress within the material, leading to matrix cracking, debonding, delamination, and ultimately mechanical failure. Fiber optic sensors do not present a similar problem, since the sensor itself is a fiber that

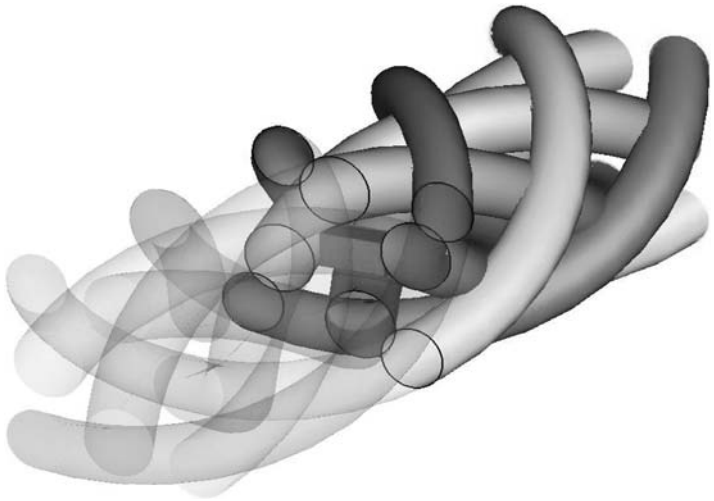

Figure 12.29 (See color insert following page 302) Illustration of a sensor embedded in a composite braid.

commingles with the other reinforcing fibers of the material. However, fiber optic sensors do not offer the diverse sensing potential of MEMS and other microsensors. More importantly, they do not present a networking option within the structure itself, which is an essential ingredient of a truly *sensing* composite, as will be discussed in greater detail below.

To address the issues associated with structural integrity, we envisage a multicomponent braid, which consists of fibers for mechanical reinforcement, metallic (e.g., copper) wires for power and communications, and polymer matrix material impregnated around periodically spaced sensor or electronics packages, that can be integrated into the composite as a single fibrous braided element (see Figure 12.29). The multicomponent braid also acts to isolate the sensor or electronics elements within a protective environment that is commensurate with the composite structure as a whole. Rather than acting as an inclusion, the sensor network is integrated directly into the fiber phase of the composite. Braiding these sensors into and along with reinforcing fibers forms a protective casing around the discontinuity that mitigates the flaws and related failure modes of embedded designs.

The resulting sensor braid is suitable for inclusion in the composite panel in one of two ways. First, it may be directly laid into the composite layup, forming an integral vein within the composite structure, the woven fiber sheets forming the basis of the material in the usual manner of laminated composites. The spacing of these sensor braids can be such that they are isolated from each other while providing the desired degree of sensing within the material. Alternatively, the braided elements may be used in creating a woven fabric that commingles the braids with further reinforcing fibers, similar to the woven fabric used in traditional laminated composites. Depending upon the desired sensor density, the electronic sublattice braid can be included at appropriate spacing in one or multiple directions as needed.

A critical issue to be addressed in forming a multicomponent braid with sensing elements is the behavior of the sensor interconnects during normal composite processing. Both the high temperature and pressures can contribute to loss of interconnects during the processing; also, if not properly managed, stresses can build during the thermal equilibration that can result in both interconnect failure and incipient failure sites.

Three-dimensional braiding has been employed in the past as a method to integrate fiber optic sensors into 3-D woven preforms of composites (El-Sherif and Ko, 1993). Our method, however, uses two-dimensional tubular braiding to create continuous fibrous braids that protect the sensor and wiring within the core of the braid. In our tubular braiding process, carriers containing spools of reinforcing fiber weave in and out of each other in a radial pattern to form a protective sheath around the sensor and wiring that feeds from a central carrier. As mentioned previously, these

braids may be woven with further reinforcing fibers to form composite fabric, or they may be placed between the layers of a laminate composite. Conventional resin transfer molding techniques such as VARTM may then be used to wet the composite fibers with thermoset polymer. Care must be taken in this step to avoid damage to the sensors due to excess pressure and in some cases temperature, if curing and/or postcuring of the polymer matrix at elevated temperature were necessary.

12.2.4.4 Data Management

As the number of sensor nodes increases, and as the data load at each sensor increases, data management becomes a key issue. If data were processed and analyzed external to the embedded network, the bandwidth needed to transport the data would grow to unrealizable levels for any reasonably sized structure. The computational requirements whether in- or ex-network become intractable as well. The size of the envisaged network of embedded sensors, even for a moderately, sized structure, will likely generate immense quantities of data that must be coordinated, interpreted, and acted upon. While optimal data fusion algorithms have been developed for small, typically unconstrained, networks of sensors (Waltz and Llinas, 1990; Goodman et al., 1997; Varshney, 1997), less is known about data fusion in networks of large numbers of sensors.

Localized processing algorithms provide a solution for the management of large data sets, and are appropriate for sensorized composites. In local processing algorithms, some primitive processing capability must be introduced to each sensor node, such that decision making in part becomes controlled by the local elements. The local processing scheme is entirely compatible with the low power, low bandwidth networks that can be *scalably* embedded in materials. Processing schemes from communication theory (Middleton, 1960; Gabrielle, 1966), specifically the FFT and decoding large block length codes, suggest that efficient and near optimal solutions can be achieved with local, hierarchical algorithms. The alternative to local processing, for example, extracting all data and performing external processing, is a computationally infeasible procedure (NP-complete); large-sized data sets cannot be used optimally (Tsitsiklis and Athans, 1985).

Any proposed method of data handling or processing will not be specifically applicable to all applications. The nature of the data or problem will generally dictate the type of solution needed.

12.2.4.5 Preliminary Results

We have undertaken some preliminary work to verify the feasibility of embedding sensors in composites. An early issue is whether the proposed sensors, as well as interconnects, can survive composite processing. As an initial test case, we embed sensors into a layup of thermally cured prepreg composite.

The DS18B20X 1-Wire digital thermometer was chosen as a demonstration sensor.[4] The DS18B20X has a 1.32 by 1.93 mm footprint, and is 0.6 mm high. A microprocessor was programmed to communicate over the micro-network. A planar substrate was chosen for the initial demonstration. The substrate was a conventional fiberglass-based printed circuit board material (FR4), 0.010 in. thick, 0.080 in. wide and 6 in. long with a $\frac{1}{2}$ oz. Cu foil overlayer. Strips with the device land pattern shown in Figure 12.30 were fabricated using a rapid PCB prototyping numerical controlled milling machine.[5] While 1-Wire devices can operate in a two conductor "parasitic" mode, a more robust three-wire configuration was selected to allow the power and communications to have separate lines, sharing a common ground. Convection hot gas solder reflow was used to connect to the substrate.

Following preliminary electronic testing of the device, it was embedded in a glass fiber-reinforced epoxy composite. Style 7781 E-glass fabric was preimpregnated with BT-250 epoxy resin supplied by Bryte Technologies, Inc. The substrate with attached sensor was embedded in the middle of eight layers of prepregged material. The layup was consolidated at 250°F for 1 h under 50 psi pressure according to the material processing specifications. The connecting wires were

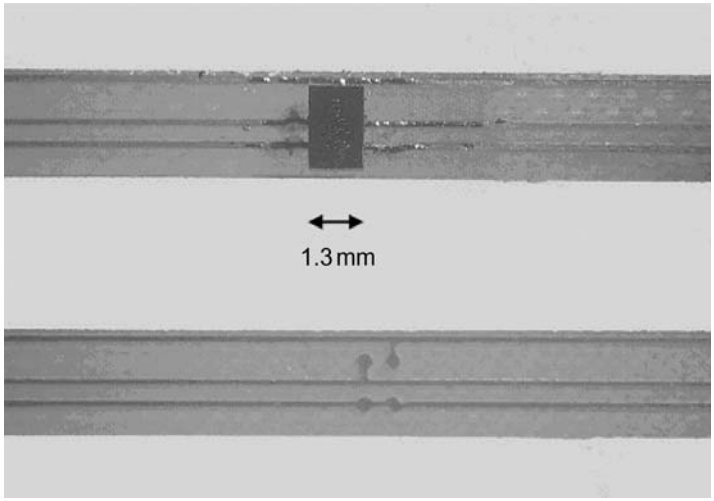

Figure 12.30 Photograph showing substrate with fabricated traces and land pattern (below) and with sensor attached (above).

passed through a silicone sealing tape that protected them from excess resin during the curing process. The sensor as embedded was demonstrated to work successfully. The 1-Wire protocol was implemented in an SX48-based microcontroller that serves as the 1-Wire master. The total network length (master to device) was about 20 cm for this proof-of-principle work.

Any sensor with a temperature-dependent output may require control or calibration of thermal effects. Repetitive reads of the DS18B20X were observed to cause a temperature increase as a result of self-heating effects in the IC. The observed temperature rise after 5 min is shown in Figure 12.31 as a function of the reading rate. Obviously, the heat capacity and thermal conduction coefficients of the particular sample determine the dynamic and ultimate steady-state temperature increase.

A 10 by 10 array of the same sensors was also fabricated on similar FR4 circuit board material. After verification of the operation of the 10 by 10 array it was embedded in an aramid fiber (Kevlar) reinforced composite panel. The panel is 15 cm by 15 cm square, and is about 2.5 mm thick. It was formed from 16 layers of aramid fabric under vacuum-assisted resin transfer molding. A two-part epoxy resin was pulled through the fabric by the vacuum action to provide complete wetting of the

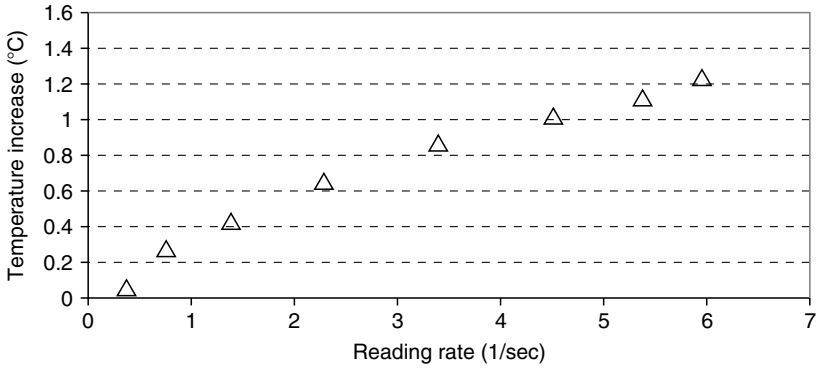

Figure 12.31 Observed temperature increase (over 5 min) of the DS18B20X as a function of reading rate.

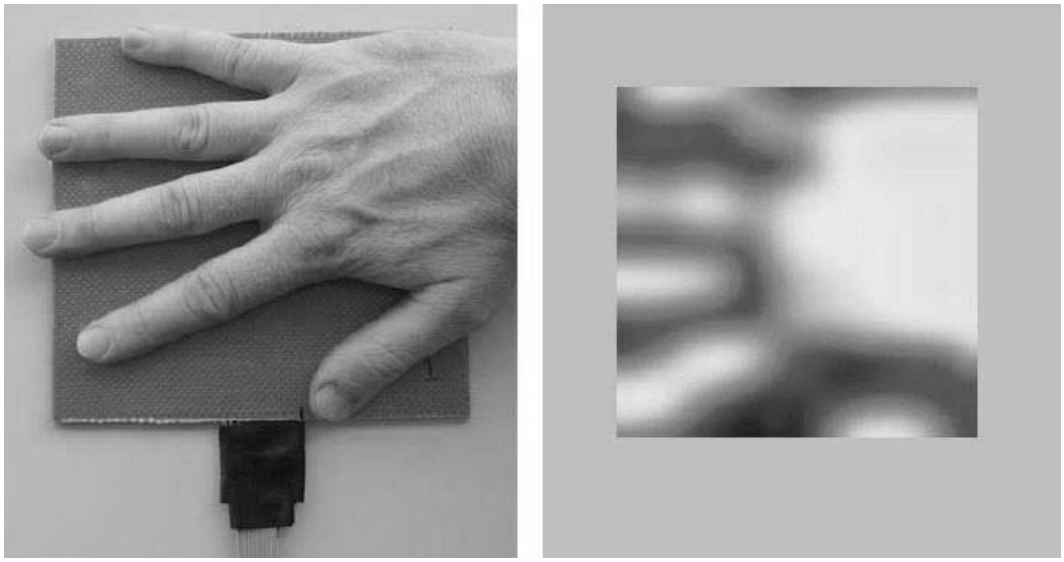

Figure 12.32 Composite panel with embedded network consisting of a 10 × 10 array of individually addressable thermal sensors. A hand is placed on the panel (left) generating a thermal image (right). The image shown is generated after about 20 sec, and represents about 3°C maximum increase over ambient.

fibers. In this case, the fabric was draped over the sensors and substrate. This panel is shown in Figure 12.32.

12.2.4.6 Sensors for Structural Health Monitoring

Continued research is necessary to successfully develop a sensor integration technology within a braided fiber component of a composite. It will be necessary to measure the mechanical properties of the embedded sensor composite in a variety of mechanical loading scenarios to determine and limit any adverse impacts on the strength of the composite. Additionally, detailed electrical design of the embedded network will need to be undertaken. If higher sensor densities are to be contemplated, the network architecture and data handling strategies will also need careful study.

The current work is focused on the implementation of a composite embedded network. As those problems are solved, it will be necessary to turn to specific structurally significant sensors to finally realize integrated structural health monitoring of composites. We expect continued progress in electronic miniaturization and power management. Smaller IC linewidths will drive the overall size of chip scale packages smaller. Current work in implementing 45° on chip interconnects also promise to reduce Si real estate demands. Higher levels of integration of MEMS-based sensors with standard IC processing will result in greater choices of microsensors to integrate into composite structures.

12.3 SUMMARY

The field of multifunctional materials is still in its infancy with regard to various functionalities that may be integrated into structural materials. With Nature as our guide the possibilities are limitless. We have presented an overview of a multifunctional composite material being developed at UCSD. This material incorporates electromagnetic, thermal management, healing and sensing functionalities into a structural composite. Integrated copper conductors resonate to provide a tuned dielectric constant and index of refraction, ranging from negative through positive values. These conductors

may also serve as resistive heating elements to provide thermal management, which may be further utilized to activate a thermal repair mechanism in a healable polymer matrix. Integrated network sensors provide *in situ* sensing and damage detection at scalable and potentially high areal density with local processing and decision making. Future work will include the fabrication of smaller scale conductive element designs to achieve EM functionality in the terahertz frequency regime. The architecture of the braided elements is being tailored to obtain optimal mechanical properties of the composite structure. We are now studying other sensing technologies, such as piezoelectrics and MEMS devices, which will interact through a network similar to that which we have demonstrated with our thermal sensors.

NOTES

1. We keep the additional numerical correction factor $-\frac{1}{2}(1+\ln\pi)$ that Pendry usually drops because we typically employ this formula for values of d and r that do not follow the assumption that $\ln(d/r)>>1$.
2. Hughes Circuits, 540 S. Pacific St, San Marcos, CA 92069–4056.
3. 1-Wire is registered by its developer Dallas Semiconductor, who has subsequently been acquired by Maxim Integrated Products.
4. Maxim Integrated Products, Inc., 120 San Gabriel Drive, Sunnyvale, CA 94086.
5. CF100 from LPKF Lasers and Electronics, North America, 28880 SW Boberg Rd, Wilsonville, OR 97070.

REFERENCES

Ageorges, C., L. Ye and M. Hou (2000). Experimental investigation of the resitance welding of thermoplastic composite materials. *Composite Science and Technology* **60**: 1027–39.

Amirkhizi, A., T. Plaisted, S.C. Nemat-Nasser and S. Nemat-Nasser (2003). *Metallic Coil–Polymer Braid Composites: I. The Numerical Modeling and Chirality.* ICCM–14, Society of Manufacturing Engineers, San Diego, CA.

Baucom, J. N., J. P. Thomas, W. R. Pogue Iii and M. A. Qidwai (2004). Autophagous structure-power systems. Active materials: behaviour and mechanics, *Proceedings of SPIE — The International Society for Optical Engineering Smart Structures and Materials, San Diego, CA*.

Bleay, S. M., C. B. Loader, V. J. Hawyes, L. Humberstone and P. T. Curtis (2001). A smart repair system for polymer matrix composites. *Composites—Part A: Applied Science & Manufacturing* **32**(12): 1767–76.

Chen, X., M. A. Dam, K. Ono, A. Mal, S. Hongbin, S. R. Nutt, K. Sheran and F. Wudl (2002). A thermally remendable cross-linked polymeric material. *Science* **295**(5560): 1698–702.

Chen, X., F. Wudl, A. Mal, S. Hongbin and S.R. Nut (2003). New thermally remendable highly cross-linked polymeric materials. *Macromolecules* **36**: 1802–07.

Christodoulou, L. and J. D. Venables (2003). Multifunctional material systems: the first generation. *JOM* **55**(12): 39–45.

Chujo, Y., K. Sada and T. Saegusa (1990). Reversible Gelation of polyoxazoline by means of Diels–Alder reaction. *Macromolecules* **23**: 2636–4.

Cox, B. N., W. C. Carter and N. A. Fleck (1994). Binary model of textile composites. I. Formulation. *Acta Metallurgica et Materialia* **42**(10): 3463–79.

Dallas, S. (2004). *Tech Brief 1: MicroLAN Design Guide*, Dallas Semiconductor.

El-Sherif, M. A. and F. K. Ko (1993). *Co-braiding of Sensitive Optical Fiber Sensor in 3D Composite Fiber Network*. SPIE — the International Society for Optical Engineering, Bellingham, WA.

Engle, L. P. and K. B. Wagener (1993). A review of thermally controlled covalent bond formation in polymer chemistry. *Journal of Macromolecular Science* **C33**(3): 239–57.

Eveno, E. C. and J. W. Gillespie Jr. (1988). Resistance welding of graphite polyetheretherketone composites: an experimental investigation. *Journal of Thermoplastic Composite Materials* **1**: 322–38.

Gabrielle, T. L. (1966). Information criterion for threshold determination. *IEEE Transactions of Information Theory* **6**: 484–86.

Goodman, I. R., R. P. S. Mahler and H. T. Nguyen (1997). *Mathematics of Data Fusion.* Kluwer, Boston.

Imai, Y., H. Itoh, K. Naka and Y. Chujo (2000). Thermally reversible IPN organic–inorganic polymer hybrids utilizing the Diels–Alder reaction. *Macromolecules* **33**(12): 4343–6.

Jakobsen, T. B., R. C. Don and J. W. Gillespie Jr. (1989). Two-dimensional thermal analysis of resistance welded thermoplastic composites. *Polymer Engineering and Science* **29**: 1722–9.

Joshi, P. B., B. L. Upschulte, A. H. Gelb, D. M. Lester, I. A. Wallace, D. W. Starrett, D. M. Marshall and B. D. Green (2002). Autophagous spacecraft composite materials for orbital propulsion. *Proceedings of SPIE — The International Society for Optical Engineering*, *San Diego, CA*.

Jud, K. and H. H. Kausch (1979). Load transfer through chain molecules after interpenetration at interfaces. *Polymer Bulletin* 697–707.

Jud, K., H. H. Kausch and J. G. Williams (1981). Fracture mechanics studies of crack healing and welding of polymers. *Journal of Materials Science* **16**(1): 204–10.

Kausch, H. H. (1983). The nature of defects and their role in large deformation and fracture of engineering thermoplastics. *Pure and Applied Chemistry* **55**(5): 833–44.

Kausch, H. H. and K. Jud (1982). Molecular aspects of crack formation and healing in glassy polymers. *Plastics and Rubber Processing and Applications* **2**(3): 265–8.

Kausch, H. H. and M. Tirrell (1989). Polymer interdiffusion. *Annual review of material science. Annual Reviews.* **19**: 341–77.

Kausch, H. H., D. Petrovska, R. F. Landel and L. Monnerie (1987). Intermolecular interaction in polymer alloys as studied by crack healing. *Polymer Engineering and Science* **27**(2): 149–54.

Ko, F. (2001). Braiding. *ASM Handbook: Composites, ASM International* **21**: 69–77.

Ko, F. K., C. M. Pastore and A. Head (1989). *Atkins and Pearce Handbook of Industrial Braids.* Atkin and Pearce, Covington, KY.

Kolinko, P. and D. R. Smith (2003). Numerical study of electromagnetic waves interacting with negative index materials. *Optics Express* **11**(7): 640–8.

Lin, M. and C. Fu-Kuo (2002). The manufacture of composite structures with a built-in network of piezo-ceramics. *Composites Science and Technology* **62**: 919–39.

Mal, A. (2004). Structural health monitoring. *Mechanics* 33 (11–12): 6–16.

McGlockton, M. A., B. N. Cox and R. M. McMeeking (2003). A binary model of textile composites: III high failure strain and work of fracture in 3D weaves. *Journal of the Mechanics and Physics of Solids* **51**(8): 1573–600.

Middleton, D. (1960). *An Introduction to Statistical Communication Theory.* McGraw-Hill, New York.

Naik, R. A. (1995). Failure analysis of woven and braided fabric reinforced composites. *Journal of Composite Materials* **29**(17): 2334–63.

Nemat-Nasser, S. C., A. V. Amirkhizi, T. A. Plaisted, J. B. Isaacs and S. Nemat-Nasser (2002). Structural composites with integrated electromagnetic functionality. Smart Structures and Materials 2002: Industrial and Commercial Applications of Smart Structures Technologies, *Proceedings of SPIE — The International Society for Optical Engineering, San Diego, CA*.

Pendry, J. B., A. J. Holden, W. J. Stewart and I. Youngs (1996). Extremely low frequency plasmons in metallic mesostructures. *Physical Review Letters* **76**(25): 4773–6.

Pendry, J. B., A. J. Holden, D. J. Robbins and W. J. Stewart (1999). Magnetism from conductors and enhanced nonlinear phenomena. *IEEE Transactions on Microwave Theory & Techniques* **47**(11): 2075–84.

Pendry, J. B., D. R. Smith, P. M. Valanjui, R. M. Walser and A. P. Valanju (2003). Comment on "Wave refraction in negative-index media: always positive and very inhomogeneous" (and reply). *Physical Review Letters* **90**(2): 9703.

Plaisted, T., C. Santos, A. Amirkhizi, S. C. Nemat-Nasser and S. Nemat-Nasser (2003a). *Self-healing Structural Composites with Electromagnetic Functionality.* ICCM-14, Society of Manufacturing Engineers, San Diego, CA.

Plaisted, T. A., A. V. Amirkhizi, D. Arbelaez, S. C. Nemat-Nasser and S. Nemat-Nasser (2003b). Self-healing composites with electromagnetic functionality. Smart Structures and Materials 2003: Industrial and Commercial Applications of Smart Structures Technologies, *Proceedings of SPIE — The International Society for Optical Engineering, San Diego, CA*.

Qidwai, M. A., J. P. Thomas, J. C. Kellogg and J. Baucom (2004). Energy harvesting concepts for small electric unmanned systems. Active Materials: Behaviour and Mechanics, *Proceedings of SPIE — The International Society for Optical Engineering Smart Structures and Materials, San Diego, CA*.

Ramakrishnan, B., L. Zhu and R. Pitchumani (2000). Curing of composites using internal resistive heating. *ASME Journal of Manufacturing Science and Engineering* **122**(1): 124–31.

Sancaktar, E., W. Ma and S. W. Yugartis (1993). Electric resistive heat curing of the fiber-matrix interface in graphite/epoxy composites. *ASME Journal of Mechanical Design* **115**: 53–60.

Santos, C., T. A. Plaisted, D. Arbelaez and S. Nemat-Nasser (2004). Modeling and testing of temperature behavior and resistive heating in a multi-functional composite. Smart Structures and Materials 2004: Industrial and Commercial Applications of Smart Structures Technologies, *Proceedings of SPIE — The International Society for Optical Engineering, San Diego, CA*.

Shelby, R. A., D. R. Smith and S. Schultz (2001). Experimental verification of a negative index of refraction. *Science* **292**(5514): 77–79.

Smith, D. R., D. C. Vier, W. Padilla, S. C. Nemat-Nasser and S. Schultz (1999). Loop-wire medium for investigating plasmons at microwave frequencies. *Applied Physics Letters* **75**(10): 1425–7.

Smith, D. R., W. Padilla, D. C. Vier, S. C. Nemat-Nasser and S. Schultz (2000a). Negative permeability from split ring resonator arrays. *2000 Conference on Lasers and Electro-Optics Europe, Nice, France, IEEE 2000 Piscataway, NJ, USA*.

Smith, D. R., W. J. Padilla, D. C. Vier, S. C. Nemat-Nasser and S. Schultz (2000b). Composite medium with simultaneously negative permeability and permittivity. *Physical Review Letters* **84**(18): 4184–7.

Smith, D. R., D. Schurig and J. B. Pendry (2002). Negative refraction of modulated electromagnetic waves. *Applied Physics Letters* **81**(15): 2713–5.

Smith, D. R., D. Schurig, M. Rosenbluth, S. Schultz, S. A. Ramakrishna and J. B. Pendry (2003). Limitations on subdiffraction imaging with a negative refractive index slab. *Applied Physics Letters* **82**(10): 1506–8.

Smith, D. R., P. Kolinko and D. Schurig (2004a). Negative refraction in indefinite media. *Journal of the Optical Society of America B—Optical Physics* **21**(5): 1032–43.

Smith, D. R., P. Rye, D. C. Vier, A. F. Starr, J. J. Mock and T. Perram (2004b). Design and measurement of anisotropic metamaterials that exhibit negative refraction. *IEICE Transactions on Electronics* **E87C**(3): 359–70.

Smith, D. R., D. Schurig, J. J. Mock, P. Kolinko and P. Rye (2004c). Partial focusing of radiation by a slab of indefinite media. *Applied Physics Letters* **84**(13): 2244–2246.

Starr, A. F., P. M. Rye, D. R. Smith and S. Nemat-Nasser (2004). Fabrication and characterization of a negative-refractive-index composite metamaterial. *Physical Review B* **70**: 113102.

Thomas, J. P., M. A. Qidwai, P. Matic, R. K. Everett, A. S. Gozdz, M. T. Keennon and J. M. Grasmeyer (2002). Structure-power multifunctional materials for UAV's. *Proceedings of SPIE — The International Society for Optical Engineering, San Diego, CA*.

Tsitsiklis, J. and M. Athans (1985). On the complexity of decentralized decision making and detection problems. *IEEE Transactions on Automatic Control* **30**: 440–6.

Varadan, V. K. and V. V. Varadan (2000). Microsensors, microelectromechanical systems (MEMS), and electronics for smart structures and systems. *Smart Materials and Structures* **9**: 953–72.

Varshney, P. K. (1997). *Distributed Detection and Data Fusion*. Springer, New York.

Veselago, V. G. (1968). The electrodynamics of substances with simultaneously negative values of [permittivity] and [permeability]. *Soviet Physics USPEKI* **10**: 509.

Waltz, E. and J. Llinas (1990). *Multisensor Data Fusion*. Artech House, Boston.

White, S. R., N. R. Sottos, P. H. Guebelle, J. S. Moore, M. R. Kessler, S. R. Sriram, E. N. Brown and S. Viswanathan (2001). Autonomic healing of polymer composites. *Nature* **409**(6822): 794–7.

Wool, R. P. (1978). Material response and reversible cracks in viscoelastic polymers. *Polymer Engineering and Science* **18**(14): 1057–61.

Wool, R. P. (1979). Crack healing in semicrystalline polymers, block copolymers and filled elastomers. *Adhesion and adsorption of polymers.* Plenum, New York **12A:** 341–62.

Wool, R. P. (1995). *Polymer Interfaces: Structure and Strength*, Hanser, München.

Wool, R. P. and K. M. O'Connor (1981a). Craze healing in polymer glasses. *Polymer Engineering and Science* **21**(14): 970–77.

Wool, R. P. and K. M. O'Connor (1981b). A theory of crack healing in polymers. *Journal of Applied Physics* **52**(10): 5953–63.

Wool, R. P. and K. M. O'Connor (1982). Time dependence of crack healing. *Journal of Polymer Science: Polymer Letters Edition* **20**: 7–16.

Wool, R. P., B. L. Yuan and O. J. McGarel (1989). Welding of polymer interfaces. *Polymer Engineering and Science* **29**(19): 1340–1367.

Xu, J., B. N. Cox, M. A. McGlockton and W. C. Carter (1995). A binary model of textile composites. II. The elastic regime. *Acta Metallurgica et Materialia* **43**(9): 3511–24.

Yang, Q. D., B. Cox and Y. Qingda (2003). Spatially averaged local strains in textile composites via the binary model formulation. *Journal of Engineering Materials and Technology* **125**(4): 418–25.

Zhou, G. and L. M. Sim (2002). Damage detection and assessment in fibre-reinforced composite structures with embedded fibre optic sensors — review. *Smart Materials and Structures* **11**: 925–39.

ACKNOWLEDGMENTS

Part of the research summarized in this chapter has been conducted at the Center of Excellence for Advanced Materials (CEAM) at the University of California, San Diego under the support of ARO/DARPA DAAD19-00-1-0525 contract to UCSD. The authors wish to thank Dr. Leo Christodoulou and Dr. John Venables of the DARPA Defense Science Office of for helpful guidance and encouragement. Research on the integration of sensing in composites is currently supported by the NSF under grant CMS-0330450. Dr. Shi-Chi Liu is gratefully acknowledged for his support and encouragement.